Electronic Properties of a Cytosine Decavanadate: Toward a Better Understanding of Chemical and Biological Properties of Decavanadates

Nada Bošnjaković-Pavlović, Anne Spasojevic - de Biré, Isabel Tomaz, Nouzha Bouhmaida, Fernando Avecilla, Ubavka Mioč, João Costa Pessoa, Nour Eddine Ghermani

Electron and electrostatic properties of a cytosine decavanadate compound from high resolution X-ray diffraction: toward a better understanding of chemical and biological properties of decavanadates

Journal:	*Inorganic Chemistry*
Manuscript ID:	draft
Manuscript Type:	Article
Date Submitted by the Author:	
Complete List of Authors:	Bošnjaković-Pavlović, Nada; Ecole Centrale Paris, Laboratoire Structures, Propriétés et Modélisation des Solides (SPMS), UMR CNRS 8580; University of Belgrade, Faculty of Physical Chemistry Spasojevic - de Biré, Anne; Ecole Centrale Paris, Laboratoire Structures, Propriétés et Modélisation des Solides (SPMS), UMR CNRS 8580 Tomaz, Isabel; Centro de Quimica Estrutural, Instituto Superior Tecnico, TU Lisbon Bouhmaida, Nouzha; Université Cadi Ayyad, Faculté des Sciences Semlalia, Physique Avecilla, Fernando; Universidade da Coruña,, Departamento de Química Fundamental, Facultad de Ciencias Mioč, Ubavka; University of Belgrade, Faculty of Physical Chemistry Pessoa, João; Instituto Superior Tecnico, Universidade Tecnica de Lisboa Ghermani, Nour Eddine; Université Paris XI, Faculté de Pharmacie; Ecole Centrale Paris, Laboratoire Structures, Propriétés et Modélisation des Solides (SPMS), UMR CNRS 8580

Electron and electrostatic properties of a cytosine decavanadate compound from high resolution X-ray diffraction: toward a better understanding of chemical and biological properties of decavanadates

Nada Bošnjaković-Pavlović,[a,b] Anne Spasojević-de Biré,[a] Isabel Tomaz,[c] Nouzha Bouhmaida,[d] Fernando Avecilla,[e] Ubavka B. Mioč,[b] João Costa Pessoa,[c] and Nour Eddine Ghermani*[a,f]*

[a] Laboratoire Structures, Propriétés et Modélisation des Solides (SPMS), UMR CNRS 8580, Ecole Centrale Paris, Grande Voie des Vignes, 92295 Châtenay-Malabry, France

[b] Faculty of Physical Chemistry, University of Belgrade, P.O. Box 47, 11158 Belgrade, PAC: 105305, Serbia

[c] Centro de Quimica Estrutural, Instituto Superior Tecnico, TU Lisbon, Av. Rovisco Pais, 1049-001 Lisboa, Portugal

[d] Laboratoire des Sciences des Matériaux (LSM) Université Cadi Ayyad, Faculté des Sciences Semlalia, Boulevard Prince Moulay Abdallah, BP 2390, 40000 Marrakech, Morocco

[e] Departamento de Química Fundamental, Facultad de Ciencias, Universidade da Coruña, Campus da Zapateira s/n, 15071 A Coruña, Spain

[f] Laboratoire de Physique Pharmaceutique, UMR CNRS 8612, Faculté de Pharmacie, 5 rue Jean-Baptiste Clément, 92296 Châtenay-Malabry, France

email :anne.spasojevic@ecp.fr

Title running head : Electron and electrostatic properties of a decavanadate

TABLE OF CONTENTS GRAPHIC

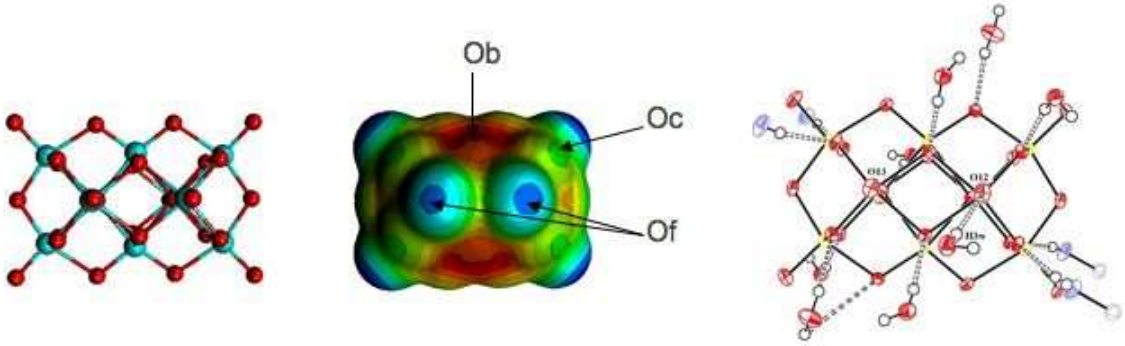

ABSTRACT

Investigation of the interactions of the polyoxometalates with peptides or proteins presents a growing interest, since the polyoxometalates have been successfully used as drugs and their biological activity has been established. The polyoxovanadates have been found able to interact with biomolecules with various and versatile activities (enzyme activator or inhibitor). However, despite the fact that such inhibitory or stimulating functions have been extensively studied not much information is available at the molecular level. A contribution to the understanding of the mechanism involved at the molecular level could be partially reached by a better knowledge of the electronic and electrostatic properties of the compound. These properties may be extracted from a high resolution X-ray diffraction experiment and derived from charge density studies. Among different synthesized polyoxometalates, we have focused our attention on polyoxovanadates due to the relative low toxicity in biological media of vanadium and the feasibility of the charge density study. In an attempt to increase the knowledge on the biochemical interactions of such polyanions, we have synthesized and crystallized a cytosine-decavanadate compound, Na_3 $[V_{10}O_{28}]$ $(C_4N_3OH_5)_3(C_4N_3OH_6)_3 \cdot 10H_2O$. We present the crystal structure, the deformation density maps, the atomic net charges and the electrostatic properties of the title compound after a multipole refinement. Some conclusions on the properties of the decavanadate (electrostatic properties, net atomic charges, hydrogen bond network) are drawn for the evidence of biological activities of this particular anion.

KEY WORDS

Electron density, decavanadate, electrostatic potential, AIM, hydrogen bonds

INTRODUCTION

Polyoxometalates (POM's) are a fascinating class of metal-oxygen cluster compounds with a unique structural variety and interesting properties, which are used in different fields. Among the different synthesized POM's, we have focused on the polyoxovanadates (POV's). The vanadium has been chosen for its relative low toxicity in biological media. Interaction analysis of vanadate and cellular proteins is difficult under physiological conditions because the aqueous vanadate species are pH, temperature, buffer and vanadate concentration dependant.[1] In biological systems, vanadium (V) containing solutions exhibits different oligomeric vanadate species in equilibrium e.g., monomeric, dimeric, tetrameric and decameric, each with different states of protonation and conformation, depending on experimental conditions. It is beleived that almost 98% of vanadium in cells is present in the vanadium (IV) oxidation state, the intracellular concentration of vanadium (V) being very low for the formation of vanadate oligomers. This is probably the reason why *in vivo* toxicological studies of vanadate oligomers are scarce. However, it is proposed that once formed, decavanadate (DV) eventually converts to the labile oxovanadates but the rate can be very slow and effectively allows DV to exists for some time under physiological conditions.[2] V half - life in the intracellular medium has been estimated to be approximately half an hour,[3] enough to allow to study its effects not only *in vitro*, but also *in vivo*.[4,5] However its presence in significant amounts can be explained by the existence of special cell compartments where vanadium can be accumulated and preserved from decomposition (protective "cage"). This can be explained by hydrogen-bonding interactions with surrounding molecules, like proteins or macrocyclic ligands.[6]

Several studies report that DV has a strong inhibitory effect on several enzymes, when compared to other oligomers:[7-9] inhibition of Ca^{2+}ATPase,[10-13] Na,K-ATPase,[14] muts ATPase,[15] myosin ATPase,[16-20] acid phosphatase A,[21] methaemoglobin reductase,[4] hexokinase, adenylate kinase and phosphofructokinase,[22] protein kinase,[23] (NADPH) oxidase,[24] aldolase,[25] ribonuclease,[26] nucleotidase,[27] phosphorylase.[28] It has also been recently reported that DV can act as an insulin

mimetic agent.[29,30] Aureliano et al. have formulated the hypothesis that mytochondria might be a target for DV species.[31] A complete review of biological activities of DV is given in a recent review of Aureliano et al. [2]

Investigations of POV's in the presence of enzymes and proteins can provide additional information on their mode of action. This research needs to proceed through combined crystallographic, spectroscopic, and enzymatic studies with mutants as well as with wild-type enzymes. Potentiometric studies have proven to be an adequate means to investigate the vanadate - peptide systems. ^{51}V NMR spectroscopy was used to determine the rates of oligoanion exchange under the physiological condition. For example, Meicheng et al.[32] have observed hydrogen bonding interactions between the 4-ethylpyridinium cation and the DV ion that involves oxygen atoms possessing two or three bonds with vanadium. Crans et al.[33,34] have extensively investigated POV-enzyme interactions. They have structurally characterized the DV - dipeptide complex. It was found that the dipeptides are connected to DV anions *via* hydrogen bonds. Very weak hydrogen bonding interactions between guanidinium ion and singly and doubly coordinated oxygen atoms in DV anions have also been observed.[35] These studies illustrate the importance of the noncovalent interactions between DV and peptides; DV interacts very strongly with positively charged proteins. Therefore, the study of POV containing organic molecules is important, particulary the role of the organic cations in the structure of the DV and understanding the direct interactions of vanadate with cellular proteins and enzymes may be an important key to reveal the physiological functions of vanadium oxoanions. Since the biological properties also result from interactions with viral enzymes or with viral cell envelopes, the understanding of these interactions at a molecular level is essential for the interpretation and the development of potent compounds with selective enzymatic affinity.

It has been demonstrated that accurate electron density can give pertinent information concerning the interactions between drug or potent drug and their biological targets.[36-41] Experimental X-ray determination of the accurate electron density in compounds containing transition metals has grown

as a major area in the past few years. Most of the progress is due to the recent availability of fast devices like area detectors which provide full and very accurate data sets in short times even for crystals with large unit-cells. The fact that deformation density studies require optimal diffraction data quality and that *3d* transition metals present special problems when refining the deformation density, because of the significantly different radial extension of the *3d* and *4s* valence orbitals, could explain that there is a very few number of papers dealing with experimental deformation density of vanadate compounds.[42-44]

Besides experimental studies, theoretical calculations have already been performed for an isolated $[V_{10}O_{28}]^{6-}$ anion.[45-48] The goal of these calculations is to investigate the electronic structure of the POV anion. As this anion may possess different protonation sites, spectroscopic and structural studies were performed in order to localize the protonation sites of the DV's.[49,50] In order to get a quantitative determination of the reactivity of the six external sites of oxygen atoms, the theoretical calculations explain and predict the behaviour of those species in case of an attack from protons or cationic groups. The possibility of predicting hydrogen bonds between polyanion and water molecules with their associated interaction energies was established. It was found that the double-linked and triple-linked oxygen atoms are those which are most susceptible of protonation owing to the basicity of these atoms compared with the terminal atoms. The topography of the electrostatic potential (EP) distribution in the accessible region of the molecules is expected to provide information concerning the approach of a reagent, either electrophilic, dipolar, or nucleophilic.

We have already studied the crystal structure and the electrostatic properties of the $(NH_4)_6 [V_{10}O_{28}] . 6H_2O$ derived from a κ-refinement.[51] In this paper, we report the crystal structure and electrostatic properties of $Na_3 [V_{10}O_{28}] (C_4N_3OH_5)_3 (C_4N_3OH_6)_3 \cdot 10H_2O$ in order to have experimental evidence of the electostatic properties derived from a co-crystal containing DV and an organic moiety, and to relate the properties derived from a charge density study to the DV biological properties observed elsewhere.

METHODOLOGY

The crystal electron density is described as a superposition of aspherical pseudoatoms according to the Hansen-Coppens formalism.[52] The deformation density maps have been clearly defined by Coppens.[53] A κ-refinement[54] has been performed: P_{val} and κ parameters for the non-hydrogen atoms have been refined. Atomic net charges are derived from the experimental monopole population (P_{val}) after a κ-refinement and referenced as to the κ charges. A quantitative investigation of the bonding can be performed by means of a topological analysis according to the Atoms in Molecules (AIM) theory.[55] Following Bader[55] and Cremer et al.[56,57] the atomic interaction may be characterized through the values of density $\rho(r_{CP})$, the Laplacian $\nabla^2\rho(r_{cp})$, the kinetic energy density $G(r_{cp})$ and the local energy density $E(r_{cp})$ at the (3,-1) bond critical points (BCP). The total energy density $H(r_{cp})$ is defined as the sum of a kinetic energy density $G(r_{cp})$ and a potential energy density $V(r_{cp})$. Abramov[58] has proposed an empirical formula: $G(r_{cp}) = \frac{3}{10}(3\pi^2)^{2/3}\rho^{5/3}(r_{cp}) + \frac{1}{6}\nabla^2\rho(r_{cp})$. The Laplacian and the energy density are related by: $2G(r_{cp}) + V(r_{cp}) = \frac{1}{4}\nabla^2\rho(r_{cp})$. The topological analysis of the electron density has been carried out using the NEWPROP program.[59,60] Experimental atomic net charges is derived from results of the topology of the charge density and referenced as to the AIM charges.[55] Further quantitative information on the electronic structures of metal atoms is obtained by *d*-orbital population analysis. Since the multipole terms in the Hansen-Coppens model[52] represent an analytical description of the asphericity of the atomic charge density distribution, the *d*-orbital populations can be calculated directly from the multipole coefficients, P_{lm} according to the linear combination reported by Holladay et al. [61] The electrostatic potential (EP) Φ(r) is computed using ELECTROS program[62] as $\Phi(r) = \sum_{atom}^{molecule} \frac{Z_{at}}{|r - R_{at}|} - \int \frac{\rho_{at}(r')}{|r - R_{at} - r'|} d^3r'$ the sum of the contributions of the positive nuclear charge Z_{at} located at R_{at} and the atomic electron density ρ_{at}.

EXPERIMENTAL

Synthesis

Heteropoly- and isopoly- anions have been prepared and isolated from both aqueous and non-aqueous solutions.[63] The most common preparative method involves acidification of aqueous solutions of simply oxoanion and the necessary heteroatoms; in many cases, it is necessary to control temperature or pH. Isolation of the polyanion from solution is generally achieved by addition of an appropriate counterion, commonly an alkali metal, ammonium or tetraalkyl-ammonium.[64]

Cytosine (0.444 g, 4.00 mmol) was dissolved in ca. 40 mL of water at 50ºC. Sodium acetate trihydrate (0.964 g, 7.09 mmol) were added. A solution of salicylaldehyde (0.84 mL, 8 mmol) in 10 mL ethanol was added drop wise and slowly, and the mixture allowed to react for 1 h at 323 K.

A concentrated blue solution of oxidovanadium(IV) sulphate pentahydrate (0.862 g, 3.4 mmol) in 2.5 mL of water was then added drop wise. The reaction mixture became dark brown, and within a few minutes heavy precipitation of a light green solid occurred, which was filtrated from the reaction mixture. This solid was most probably a mixture of the oxidovanadium(IV) bis-complex with salicylaldehyde ($V^{IV}O(Sal)_2$) and the oxidovanadium(IV) Schiff-base complex of salicylaldehyde and cytosine: [$V^{IV}O$(Sal-Cyt)X]; the identity/amount of anion X was not determined.

The filtrate was kept in a closed vessel at 279 K. A few weeks later reddish crystals suitable for X-ray diffraction analysis were separated from the liquid.

Data collection, data reduction and refinements

Crystallographic measurements were carried out at 210 K on a Siemens SMART CCD 1K diffractometer using Mo Kα radiation. This temperature was chosen due to the fact that we have observed a phase transition occurring below 200 K from the $P\bar{1}$ (centrosymmetric) to the P1 space group (non-centrosymmetric). Resolution of the structure at 100 K does not allow us to get of a good

quality results (localization of the all hydrogen atoms) because, in the P1 space group, the number of parameters is too high. A total of 38 400 frames were recorded with five different exposure time per frame (2, 5, 10, 20, 30 s) depending on the 2θ detector position; 221 309 reflections were collected. The absorption correction was applied using SADABS.[65] Data were sorted and merged using SORTAV,[66] giving 28 757 independent data up to a resolution of $[\sin\theta/\lambda]_{max} = 1.11$ ($\theta_{max}=75°$). The structure was solved by SIR92.[67] $Na_3[V_{10}O_{28}](C_4N_3OH_5)_3\ (C_4N_3OH_6)_3 \cdot 10H_2O$ crystallizes in the centro-symmetric space group $P\bar{1}$ at temperature > 210 K. All structural calculations were performed by using the SHELXL-97,[68] program of the WINGX software package.[69] All atoms, except the hydrogen ones, were refined by using anisotropic thermal parameters. Thermal ellipsoid plots were obtained using the program ORTEP3.[70] The Hansen-Coppens multipole formalism,[52] implemented in the MOLLY program, was used for multipole and κ refinements.[54,71] Table 1 gives the experimental details of the single crystal experiment.

The radial terms used for V atoms were simple Slater functions, $R_{nl}(r) = Nr^{nl} \exp(-\xi_l r)$, n = 4 and ξ = 5.99 $bohr^{-1}$ (for l = 1 to 4). The multipole terms up to hexadecapole are included for the vanadium, up to octapole for nitrogen, carbon and oxygen, and up to dipole for hydrogen atom. The local atomic frames for multipoles are given in Supplementary Material. The atomic core and valence scattering factors were taken from International Tables for X-ray Crystallography.[72] The core electron configuration was assumed to be He core for O, N and C and Ar core for V.

It is well established[71,73-75] that *3d* transition metals imply some difficulties when refining the deformation density because of the significantly different radial extension of the *3d* and *4s* valence orbitals. In view of these problems, it is a common practice to treat the *4s* density as "core" density.[76] Therefore, we have tried different models. Models based on the $4s^2 3d^3$ electron configuration were initially examined, but gave chemically unrealistic populations; those based on the $4s^0 3d^5$ configuration gave significantly high residuals in the density maps. The final model used was based on the $4s^0\ 3d^3$ configuration, where V^{2+} possesses 18 core electrons. In order to conserve the electron-neutrality, we have attributed the formal charges as follows: $[Na_3]^{3+}\ [V_{10}O_{28}]^{6-}\ [(C_4N_3OH_5)_3]^0\ [(C_4N_3OH_6)_3]^{3+} \cdot 10H_2O$. In this approach, we have not authorized a charge transfer

between the different ions of the compound. In order to minimize the number of refined parameters, we have imposed chemical constraints on water molecules: same populations and κ's for O and H respectively. Reliability refinement factors are given in Table 1.

RESULTS AND DISCUSSION

Selected interatomic distances of covalent and non-covalent interactions and topological analysis features are given in Tables 2, 3 and 4; *d* orbital populations are reported in Table 5. Net atomic charges and EP are given in Tables 6 and 7. Figure 1 gives the labeling of the different atoms in the crystal structure. After the multipole refinement, the residual deformation electron density maps of the title compound are presented in Figure 2. The absence of significant peaks and holes of residual density indicates that the multipole model refinement is satisfactory. The maximum random errors according to Rees' formulism[77] is 0.0675 e.Å^{-3}. The same trend is observed for the cytosine molecules, which, however, exhibit a significant accumulation of charge density around the N1c, C6c and C2c. This poor quality is due to a local disorder leading to high values of thermal parameters which have been observed for these atoms.

Crystal structure

The X-ray structural analysis reveals that the asymmetric unit of the title compound is composed of one half of a DV anion, three molecules of cytosine, one and half of sodium and five water molecules. DV is not protonated in the title compound, while in other crystal structures they could be protonated according to the formula $[V_{10}O_{28}H_x]^{(6-)-x}$ where x = 1-5. [78]

The $[V_{10}O_{28}]^{6-}$ anion is formed by ten slightly distorted edge-sharing VO_6 octahedra building a very compact entity. In the title compound, this entity is centrosymmetric and built by only five crystallografically independent VO_6 octahedra with approximate D_{2h} (*mmm*) symmetry (Figure 1). The vanadium atoms are not in the geometric center of the octahedron but they are closer to the

vertex occupied by the terminal oxygen atoms. Owing the complexity of the structure, it is necessary to precisely characterize the different environment of oxygen and vanadium atoms. If we classify the oxygen atoms according to their vanadium coordination, four types of oxygen atoms are involved in this compound (Figure1a). The first type corresponds to oxygen atoms bonded to only one vanadium atom (O1x). The second type corresponds to oxygen atoms shared between two vanadium atoms (O2x). The third type are those shared between three vanadium atoms (O3x). The fourth type of oxygen atoms, have a sixfold coordination with vanadium atoms building an almost regular VO_6 octahedron (O6x). Considering now the different vanadium atoms, there are three types of vanadium atoms: the first type (type I), presents two V-O2x, two V-O3x and two V-O6x bonds; the second type of vanadium atoms (type II) presents four V-O2x, one V-O1x and one V-O6x bonds; the third type of vanadium atoms (type III) presents two V-O2x, two V-O3x, one V-O1x and one V-O6x bonds. In order to compare all V-O distance values with those found in literature (experimental and theoretical data), we have classified oxygen atoms in subtypes according to new labels (Figure 1b). Type **a** concerns oxygen atom O6x, type **b** is O3x atoms, type **c** concerns O2x connected to one VII vanadium atom and one VIII vanadium atom, type **d** concerns O2x atoms connected to two VII vanadium atoms, type **e** concerns O2x connected to one VI vanadium atom and one VII vanadium atom, type **f** concerns O1x connected to VIII vanadium atom and type **g** concerns O1x connected to VII vanadium atom.

In order to compare the interatomic distances of the title compound with the literature, we have examined the organic / organometallic Cambridge Structural Database (CSD).[79] We have found 37 data for 33 $[V_{10}O_{28}]^{6-}$ structures with agreement factor R less than 10%.[80] A search in the Inorganic Crystal Structure Database (ICSD)[81] has given 44 $[V_{10}O_{28}]^{6-}$ structures with agreement factor R less than 10%.[82] The longest interatomic distance is V-Oa: 2.0781(6) Å < V-O < 2.3324(6) Å. The shortest distance is V-Og: 1.6115(6) Å < V-O < 1.6200(6) Å. Interatomic bond distances and angles observed for the $[V_{10}O_{28}]^{6-}$ unit of the title compound exhibit a geometry which is quite similar to those found in previously reported structures of DV salts or co-crystals (Table 2). The interatomic distances V-Of or V-Og observed for the title compound are slightly longer than those observed in

the literature. This difference may be due to the crystal packing effect, because the oxygen atom involved in this bond is a mono-coordinated O1x oxygen atom and could be more affected by the hydrogen-bond network. Therefore, one can consider that DV is a very rigid entity for which the interatomic distances are almost independent of the non-covalent interactions.

The asymmetric unit of the title compound contains three different molecules of cytosine (Figure 1c). The cytosine C is not protonated and is neutral. The cytosinium B is protonated, and hydrogen atom H2b is bonded to N3b leading to a charge of +1e for the molecule. The cytosinium A is protonated, a half of hydrogen atom H2a is bonded to N3a, with a charge of +0.5e. This hydrogen lies on the crystallographic center of symmetry. One can remark (Table 3) that some interatomic distances in cytosine C (C2c-O2c, C6c-N1c) deviate significantly from the corresponding distances in cytosinium A and cytosinium B. A poor resolution for the cytosine C is observed, due to high thermal anisotropic Uij values, mainly located on N1c and C6c. We have compared the distances for protonated cytosinium B (with H atom on N3b) with corresponding molecules of cytosinium, and retrieved from CSD bases 18 data extracted from 14 different structures containing cytosinium cations.[83] The geometry is quite similar to those found in previously reported structures of cytosine. As was shown in previous studies,[84-86] the protonation of the cytosine molecule induces a modification of the bond length. Not unexpectedly, the N3-C bonds of the protonated N3b nitrogen atom are slightly longer than those of the nitrogen atom N3c that acts as a hydrogen acceptor. Accordingly, both N3b-C4b and N3b-C2b bond lenghts are longer than those of N3c-C4c and N3c-C2c (1.354(1) *versus* 1.351(1) Å and 1.365(1) Å *versus* 1.357(1) Å, respectively). Furthermore, the C2-N3-C4 angle around the protonated N3b is slightly greater (0.2°) than those of the non-protonated N3c (122.26° *versus* 122.01°). Thus, as expected, the difference between the angle in the protonated (cytosinium) and the non-protonated molecule (cytosine) are sensitive to the protonation (Δ_{B-C}(N3-C4-C5)=-1.5°) and Δ_{B-C}(N4-C4-C5) =+1.6°). All these experimental values exhibit the same trend founded in previous theoretical DFT study[85] and experimental works.[84,86]

The asymmetric unit also contains two sodium atoms. Both sodium atoms (Na1 and Na2) are in octahedral coordination: Na1 is surrounded by four water molecules and two oxygen atoms

belonging to DV (O12) while Na2 is surrounded by four water molecules, one DV oxygen (O13) and one oxygen belonging to cytosine O2a (Figure 1d). The oxygen atom involved in these bonds belongs to different molecules, anions or cations, implying that the influence of environmental atoms and hydrogen-bonds on interatomic distances is different and consequently the Na-O distances are in a wide range. The Na-Ow distances are in the range from 2.3562(7)Å to 2.4031(8) Å while the other Na-O distances belongs to a wider range (2.4489(7)Å to 2.7999(7) Å). The interatomic distances retrieved in the ICSD base for nine compounds[87] give Na-Ow distance from 2.293Å to 2.647Å and Na-O distances (O not belonging to a water molecule) from 2.290Å to 2.469 Å. The Na-O distances observed for the title compound are slightly longer.

Crystal packing

The crystal structure of the title compound is stabilized by an extensive network of hydrogen bonds which involve the DV anions, the cytosine and the water molecules. Table 4 reports the most significant hydrogen bond features according to the usual criterion (d(D···A) < 3.5Å). Symmetry codes used in the text are defined in caption 4. The structure contains several varieties of intermolecular interactions such as O-H···O, N-H···O, N-H···N, C-H···O and O-H…N. The strongest interaction in DV anion is of Ow-Hw···O type. The O1w'-H1w'···O32 is the shortest interaction (1.6924(5)Å) followed by O2w-H2w'···O20$^{(v)}$ (1.7049(6) Å) and O4w-H4w'···O31$^{(x)}$ (1.7583(5)Å). There is a strong hydrogen bonding interactions between bridging oxygen atoms O2x of the DV anion and the N4 atoms of the cytosine. The shortest distance 1.8536(5) Å is found for bond N4b-H4b···O24$^{(viii)}$, followed by N4a-H4a···O23$^{(i)}$ (1.8678(6) Å) and N4c-H4c···O22$^{(iii)}$ (1.8798(5) Å). The water molecules interact with the DV and the cytosine *via* hydrogen bond, as expected.

Hydrogen bonds occur naturally between nucleic acid bases of the purine and pyrimidine type (cytosine) and that is of great biological importance for secondary structures of deoxyribonucleic acid (DNA) and ribonucleic acid (RNA).[86] The cytosinium - cytosine dimer $[(Cyt)_2H]^+$ (Figure 1c)

is the most simple model compound to mimic the hydrogen pattern of cytosine in nucleosides and nucleotides. Two molecules of cytosine A are connected over the three strong hydrogen bonds forming a dimeric cation cytosinium - cytosine, namely two terminal N4-H···O (N4a···O2a$^{(i)}$ =2.841(1)Å and N4a-H3a-O2a$^{(i)}$ =177.12(6)°) and a central N3-H···N3 (N3a···N3a$^{(i)}$ =2.838(2)Å and N3a-H2a-N3a$^{(i)}$ =167.72(2)°. In this dimeric cation, the terminal N4a-H3a···O2a hydrogen bonds are identical. The hydrogen atom of the central N3a-H2a-N3a hydrogen bond is disordered over two equally occupied positions related by an inversion center. Two molecules of cytosinium B and C are connected *via* three strong hydrogen bonds. The central hydrogen bond is N3b···N3c (N3b···N3c$^{(ii)}$ = 2.816(1) Å and N3b-H2b-N3c$^{(ii)}$ = 173.39(5)°). The two terminal N4-H3···O2 hydrogen bonds are different, a weaker (N4b···O2c$^{(ii)}$ = 2.874(2) Å) and a stronger N4c···O2b$^{(ii)}$ = 2.756(1) Å) one. This is expected because protonation implies different bond distances and bond angles (Table 3). We have observed a difference in the hydrogen bonds in cytosine A, B and C, in the N1 - C6 region. The hydrogen bonds which exist in cytosine C (C5c-H5c···O22$^{(iii)}$, N1c-H1c···O2w) are longer than those present in cytosinium B and A (2.6819(5) *versus* 2.0702(6) and 2.2430(7) and 2.288(1) *versus* 1.7519(7) and 1.7006(7), respectively. Hydrogen bonds which exist in cytosine C (C5c-H5c···O22$^{(iii)}$, N1c-H1c···O2w) are longer than in cytosine B and C. The summation of d(H…A) interatomic distances for each cytosine, gives a quantification of the strength of the hydrogen bond network and clearly indicates that cytosine C is not stabilized with strong hydrogen bond (Σ_C [d(H…A)] = 9.267 Å), compared to the two other cytosine molecules (Σ_A [d(H…A)] = 8.625 Å, Σ_B [d(H…A)] = 8.352 Å). This is in agreement with the thermal parameter values which are higher for cytosine C.

In order to describe the extensive hydrogen bond network, one can first examine, the connection network built by DV anion to the rest of the structure. The DV anions are connected *via* oxygen-sodium-oxygen chains in the (001) plane (Figure 3). In the crystal packing, Na2 interacts with O13 of DV and Na1 interacts with O12 forming a layered structure with O13-Na2-Na2-O13 and O12-Na1-O12 chains. It means that each DV anion is connected to four neighboring DV anions. As it is

shown in Figure 3, the DV are located between these layers (Na1-Ow5-Na2-Ow2-Na2-Ow5-Na1 chain). The Na2 sodium cations are connected *via* two bridged Ow2 atoms and Na1 and Na2 *via* Ow5 atom. The shortest contact between two different layers corresponds to Na2…$Na2^{(x)}$ distance (3.5830(8) Å). Then, each layer is bonded to cytosine A *via* Na2 cation. Na2 atoms serve to link adjacent DV clusters to form infinite chains. In an other direction, the anions are connected *via* hydrogen bonds (medium and weak) with cytosine B and cytosine C. DV are located between these organic layers and are connected *via* hydrogen bonds (medium and weak) with cytosine B and cytosine C. The strongest hydrogen bond is N4b-H4b···$O24^{(viii)}$ with $d_{(H-A)}$ =1.8536(5) Å and then N4c-H4c···$O22^{(iii)}$ with $d_{(H-A)}$ = 1.8798(5) Å. Other hydrogen bonds exhibit distance ($d_{(H-A)}$) greater than 2.0 Å.

Description of covalent bonds in DV anion

Static deformation density maps for horizontal and vertical XZ and YZ planes are represented in Figure 4. As expected, there is a significant charge accumulation on the shorter V-O bond. For the longest bond we do not observe any deformation density. The deformation density maps display regions of electron density accumulation around all vanadium atoms. These accumulations are oriented toward the Oa atoms. Since V-Oa distance are the longest V-O bond in the cage (yellow color in Figure 4), the density accumulations can be interpreted as the counterpart of the charge depletion occurring along the opposite and shorter V-O bonds (red color). Differences in static electron density maps in the vicinity of oxygen atoms are well expressed. Around the O22 oxygen atom (Figure 4a) we see, symmetrically distributed, an electron density accumulation in the direction of the bonds while in the vicinity of the O21 and O27 atoms, the electron density is asymmetrically shared. This is an expected result because all the vanadium atoms are not in the same environment. O22 atom is connected to two V atoms (V3 and V5) which are in the same environment, having a V-O distance of 1.8871(6) Å and 1.8795(6) Å, respectively. Therefore, we can observe a symmetrical density accumulation around O22 (Figure 4a). As it is shown in Figure 4a, O27 and O21 atoms are

located between two different types of V atoms; in this case, the charge accumulation is in the direction of the shortest bond (O27-V4 (1.6848(5) Å) and O21-V4 (1.7059(6) Å)). The highest electron density peaks (Figure 4b) are found between V1-O13 followed by those in V2-012 because the distance V1-O13 (1.6189(6) Å) is shorter than the V2-O12 distance (1.6230(6) Å). We have found for O61 atom (Figure 4a) a practically spherical electron distribution, which is in a good agreement with the theoretical calculation results.[45,46] The main differences could be attributed to the hydrogen bonding network. The deformation density is symmetrically distributed in the direction of the bonds due to very similar distances (O31-V2 = 2.0040(5) Å and O31-V1 = 2.0205(5) Å; O32-V1 = 1.9981(6) Å and O32-V2 = 2.0268(6) Å). Additionally, the lone pairs of the mono-coordinated oxygen atoms (O1x) are clearly visible.

Topological parameters of the electron density for the (3,-1) BCP′s of DV containing bonds are given in Table 2. All V-O bonds are characterized by a very large positive curvature at the BCP along the direction of the bond path (λ_3). The value of Laplacian$\nabla^2\rho(r_{cp})$ trace is largely dominated by λ_3 and therefore is positive for the whole range of V-O distances. It has been established that the positive values of $\nabla^2\rho(r_{cp})$ are characteristic of "closed-shell″ interactions governed by the contraction of the charge density toward each of interacting nuclei.[88] As it is also shown in table 2, $\rho(r_{cp})$ values range from 0.324 eÅ^{-3} for the longest V-O bond (V3-O61 = 2.3324(5) Å) to the relativelly high value of 1.789(6) eÅ^{-3} for V1-O13. The $\nabla^2\rho(r_{cp})$ value ranges from 4.36 to 30.96 eÅ^{-5}. Correlation between experimental and theoretical data is very good, except $\rho(r_c)$ value for VII-Od. This is not surprising because the distance VII-Od[46] is 1.831Å compared to our experimental result of 1.8871(6) Å. We observe (Figure 5) that $\rho(r_{cp})$ at the BCP is a decreasing function of the interatomic distances. The topological results fit quite well with the classification of the oxygen types and the vanadium types in the DV anion. The dispersion of the data is very small, leading to a quantitative agreement. Aditionnaly, d_1+d_2 is always very close to the interatomic distance, except for three bonds V3-O20, V3-O22 and V5-O22; the position of the BCP is generally at the middle of the bond, except for the shortest V-O distance where larger discrepancies are observed. The total

energy density $H(r_{cp})$ according to the Abramov formula[58] has also been calculated and presents a quite good behavior leading to significant energy for short V-O bonds.

The analysis of the total density through the existence of the BCP and the analysis to the deformation density lead to similar results and give the first experimental description of V-O bonds in a POV entity.

Description of hydrogen bonds

Topological analysis of the charge density is also a very useful tool for the characterization of hydrogen bonds.[89] It is extremely interesting to compare accurately the results of the topology and the determination of the existence of hydrogen bonds using simple geometrical parameters (d(D…A) < 3.5 Å) (Table 4). The number of significant hydrogen bonds decreases from 37 to 20. As expected, all hydrogen-bond critical points are of (3,-1) type. Hydrogen bonds are considered as closed-shell interaction, because they display $\nabla^2\rho(r_{cp}) > 0$ and small $\rho(r_{cp})$ values. The O-H···O and N-H···O interactions are found to be the strongest and present higher $\rho(r_{cp})$ value than N-H···N and C-H···O, which are very weak interactions. The O1w-H1w'···O32 and N1a-H1a···O4w are the two shortest hydrogen bonds having the highest $\nabla^2\rho(r_{cp})$. The $\rho(r_{cp})$ values for all types of bonds are in the range of $\rho(r_{cp})$ magnitudes previously reported for this kind of bonds.[90] $\rho(r_{cp})$ expresses an exponential function of the interatomic distances. The same trend is observed for the $\nabla^2\rho(r_{cp})$ despite the fact that some points are slightly out of the curves. We have observed an exponential behavior of the eigenvalue λ_3 versus d(H···O) in all D-H···O interactions. The correlation between the positive curvature λ_3 and the interatomic distance for our result is especially excellent ($y = 387.2\ e^{-2.34x}$, $R^2 = 0.933$) and in a quantitative agreement with the results obtained previously)[90] ($y = 245.7\ e^{-2.11x}$, $R^2 = 0.925$).

The O-H…O hydrogen bond type. We have found BCP's for the eight O-H…O interaction for which d(D…A) < 3 Å and D-H…A angle > 150° (Table 4). For this hydrogen bond type, D-H…A

angles and d(D…A) distances correspond to a criterion coherent with the existence of the BCP. These Ow-Hw…O bonds exhibit various electron accumulations from strong (d(H…A) = 1.6924(5)) to weak bonds (d(H…A) = 2.9904(6) Å). Observation of the static deformation maps indicates that the accumulation (number of contours at the point intersecting the bond) of the lone pair directed toward the hydrogen of the water molecule is clearly a function of the interatomic distance d (H…A). The density peak height of the lone pair is in reasonable agreement with the d(H…A) (Figure 6a,b). The height of the Ow-Hw deformation density peaks remains in the range of 0.5 to 0.6 e.Å^{-3}, while for a same d(Hw…O) the peak height of the static deformation density involved in the interaction could vary within three contours. This clearly indicates that the deformation density of the lone pair is sensitive to other parameters such as the coordination oxygen atom polyhedra (number of vanadium atoms or hydrogen bonds). Nevertheless, the shortest O…H distance ($d_{H1w'...O32}$ = 1.6924(5)Å) exhibits the highest density peak. The lone pair electron density peak height (maximum contour level of the lone pair) is 0.5 e.Å^{-3} in agreement with the highest $\rho(r_{cp})$ and $\nabla^2\rho(r_{cp})$ values observed at the BCP. In that case, oxygen lone pair is oriented toward the hydrogen bond (Figure 6a). On the contrary, the oxygen lone pair of O25 is shifted between the two O-H…O hydrogen bonds in the case of bifurcated hydrogen bonds (Figure 6b).

The N-H…O hydrogen bond type. We have found BCP's for the eight N-H…O interactions, for which d(D…A) < 3 Å and D-H…A angle > 160° (Table 4). These hydrogen bonds only concern the oxygen atoms of coordinence 2 with the vanadium atom. The observation of the electron deformation density maps reveals the following remarks: i) the intensity of the lone pair is less pronounced than in the O-H…O bond for a similar A…H distance, ii) the H-N deformation bond exhibits a more delocalized deformation density cloud than the corresponding one in the Ow-Hw bond (Figure 6c). Oxygen atom O24 is involved in one strong bond, O24$^{(viii)}$, H4b and N4b, with $d_{H\cdots A}$ =1.8536(5) Å, but the oxygen lone pair is shifted toward N-H…O hydrogen bonds. O22 presents an interesting behavior; the strongest hydrogen bond is N4c-H4c…O22$^{(iii)}$, with $d_{H\cdots A}$ =1.8798(5) Å, but the oxygen lone pair is clearly in the direction of the H5c hydrogen. That feature

means that the N-H…O interaction is not enough strong to induce a shift of the oxygen lone pair. On the opposite, the O-H…O contacts are exhibiting strong interaction. We can conclude that the O-H…O interaction is stronger than the N-H…O one. Moreover, the lone pair exhibits higher contours measured at the maximum of the lone pair (0.5; 0.3; 0.4 e.A^{-3} for the O-H…O bond) and (0.2; 0.3; 0.3 e.A^{-3} for the N-H…O bond).

The C-H…O hydrogen bond type. The C-H…O bond belongs to the category of weak or very weak hydrogen bonds.[91] For only three C-H…O hydrogen bonds, we have found a BCP. The $\rho(r_{cp})$ and $\nabla^2\rho(r_{cp})$ values for these bonds are very small and characteristic of weak hydrogen bonding.[92] It has been already noticed that it is difficult to observe electron density deformation for such a bond. This trend remains verified for the C-H…O bonds in our compound. That observation does not indicate that there is no interaction but this interaction is not detectable using the tool of the static electron deformation density. One can take the example of the O10 (Figure 6e) where two medium hydrogen bonds are represented: C5b-H5b…$O10^{(vi)}$, with $d_{H\cdots A}$ = 2.0702(6) Å and C5a-H5a…$O10^{(i)}$, with $d_{H\cdots A}$ = 2.2430(7) Å. Due to the large space available in the vicinity of these atoms, the number of multi-furcated H-bond is high. The oxygen atom is connected to three C-H…O bonds of short or medium distances. Therefore the lone pair remains almost in the opposite direction of the V-O bond. For the weak hydrogen bond the trend is less pronounced. Nevertheless, the shortest contact C5b-H5b…$O10^{(vi)}$ is not characterized by a BCP. This is not surprising due to the fact that it possesses a small D-H…A angle (98.22(6)°). The discrepancy between the bonds which present a BCP and those not displaying a BCP is consistent with the increasing interatomic distances, but the separation at d(H…A) = 2.68 Å is not straightforward.

d-orbital populations of the vanadium atoms

Holladay et al.[61] have demonstrated that a linear combination of the multipole population used in the pseudo-atom model,[52] depending of the symmetry used in the refinement lead to an experimental

determination of the *d*-orbital populations. These determinations could give quite good results, at least a quantitative agreement between experiment and theory. This was, for example, the case of a chromium complex[93,94] or other metal transition complexes.[61,95] Nevertheless experimental determination of the *d*-orbital population is rarely extracted from the multipole refinement and from our better knowledge no such experimental determination has never been published concerning a vanadate compound. metal coordination are slightly distorded octahedra, therefore we have chosen to refine the vanadium in the symmetry 1 leading to P_{lm} parameters (l=0, 2, 4) in agreement with Holladay et al.[61] For all V atoms, z axis is chosen in the direction of the closest atom, and the x axis toward the second closest atom. We have determined for each vanadium atom the *d*-orbital population (Table 5). Total *d*-orbital population analysis is coherent with an oxidation state for the V atoms of +2 in the $4s^0d^x$ configuration (x varying from 3.03 for VI to 3.20 for VII and VIII). The *d*-orbital population analysis is in good agreement with the features observed in the crystal structure, deformation density maps and topological analysis. Since a high charge concentration and higher ρ value is found on the shorter V-O bond**,** the highest population value is found in the d_{z2} orbital for VII and VIII atoms. The highest population for d_{x2-y2} orbital is found for V1 and V2. For V4, d_{x2-y2} in the plane O21-V4-O31 and d_{xz} which is along the bond V4-O21 exhibit the highest populations.

Atomic net charges

A κ-refinement has been carried out without charge transfer between cytosine molecules and DV anion, therefore only separate and comparative discussions on each entity make sense. A final refinement cycle has been performed without restraints on charge tranfer leading to similar results. Nevertheless, we will only discuss the results without charge transfer. The κ coefficients, experimental atomic net charges (derived[51] from different methods on the two available $(NH_4)_6[V_{10}O_{28}] \cdot 6H_2O$ compounds) and data from theoretical calculation[46,48] of the DV anion are compiled in Tables 6 and 7. The values are in good agreement with those determined from a κ–refinement. As expected, some differences are found between charges derived from the κ–refinement and from AIM

analysis of the experimental model density. According to the results of the κ-refinement, the vanadium atom carries an average positive charge of +1.80 *e* and a common κ parameter value of 1.04. The AIM vanadium atom charges are less positive than monopole charge (+1.60 *e versus* +1.80 *e,* respectively). In comparison, vanadium κ-charge equal to +1.6(1) *e* was reported for ammonium-DV and vanadium charge equal to +2.0(1) *e* was reported for an isolated DV anion (in an ideal D_{2h} symmetry) from theoretical calculations[46] and a value of +1.80(1) from PACHA theoretical calculation was reported by Henry.[48] In the polyanions, the internal V4 have the highest charges, whatever the method, which is in good agreement with the results from theoretical calculation.[46] The DV oxygen atom electron densities are slightly expanded (κ ≤ 1.0). For the oxygen atoms, the AIM charges are less negative than the monopole charges derived from the κ–refinement (from –0.57 *e* to –0.92 *e versus* –0.65(5) *e* to –1.08(5) *e* respectively). The Mulliken population analysis for an isolated polyanion, deduced from *ab initio* SCF theoretical calculations, indicates that the oxygen atomic net charges are in the range –0.7 *e* to –1.3 *e*.[46] The PACHA calculations[48] give oxygen charges varying from –0.56 *e* to –0.87 *e*. The negative charge on oxygen atoms consistently increases with the number of connected metal atoms. This trend is both observed in experimental and theoretical studies. Generally, net atomic charges derived from experimental and theoretical densities are in good agreement, despite the fact that the theoretical calculations are based on an isolated molecule. Nevertheless, the AIM analysis gives a more rigorous definition of the charges of the atoms in molecules, thus providing a more reliable framework for comparison between molecules and between experiment and theory.[95,96]

Electrostatic potential

In order to obtain information on the potent reactivity of the compound, it is useful to color with the EP values the reactive surface of the molecule; the most nucleophilic molecular regions correspond to the most negative EP. The experimental EP can be calculated at the final step of the three refinements (the κ-refinement, the multipole refinement and using the AIM charges). The EP values

at the 3D isodensity surface (0.007 eA^{-3}) of the DV anion are shown in Figure 7 (first column) using the maximum color scale for the EP values on the molecular surface; the blue region correspond to -4.9 eA^{-1} and the red value to –8.7 eA^{-1}. In order to have a complete picture of the electrostatic properties of the DV in the vicinity of the oxygen atoms, we have reported in Table 7 the experimental and the theoretical EP projected at the molecular surface of the DV anion in different environments or using different models.

The EP on the surface is negative on the whole molecular surface of DV, as it is expected for an anion. Some differences are found between the values from the κ-refinement, from the multipole refinement and from AIM charges. The greatest differences between the two EP determinations are found in the vicinity of the Ob oxygen sites which are involved in strongest hydrogen bond (–8.7 eA^{-1} from multipole refinement *versus* –8.2 eA^{-1} from κ-refinement, respectively). The absolute values obtained from the multipole refinement are generally higher that those obtained from the κ-charges. According to the fact that the multipole model is closer to the reality than the κ one, the EP values obtained from the multipole refinement will be only discussed in the following paragraphs.

The value of EP found in the vicinity of oxygen atoms are in the following order: Ob (-8.7 eA^{-1}) < Oe (-7.4 eA^{-1}) < Oc (-7.2 eA^{-1}) < Od (-6.9 eA^{-1}) < Of (-6.2 eA^{-1}) < Og (-5.8 eA^{-1}). Previous theoretical calculations on an isolated $[V_{10}O_{28}]^{6-}$ anion[47-49] were used to predict the protonation sites in relation with the relative oxygen atom basicities. The authors have found that the most negative region on the EP is in the vicinity of the Ob and Oc atoms. It means that Ob and Oc oxygen atoms are more involved in electrostatic interactions and hydrogen bonds. Our experimental EP results confirm the theoretical predictions. These very close values obtained on two different compounds clearly indicate that the properties obtained experimentally at a molecular level are transferable from an anion in a given environment, to an anion in another environment. For the values concerning the vanadium atom, it could be expected that the environment (such as non-covalent interactions) do not affect the vanadium atom, which is not directly at the molecular surface of the anion. Therefore, concerning the vanadium atom in a DV compound, we can note: i) we have experimentally determined the *d*-orbital population, the values could be taken as transferable. Hence, on the one

hand, we have observed from the comparison of the five vanadium that there is a real correlation within the distorded octahedra (in interactomic distances, and consequently in static deformation density and topology analysis), and on the other hand, we have observed that the DV anion remains geometrically almost invariant with respect to non-covalent interactions. ii) We have determined the net atomic charge values from different methods on different species. There is a quantitative agreement between the same partitioning method used for different anions and an agreement between different partitioning method for the same anion. Therefore one can also conclude that for a chosen partitioning method (here a κ-refinement) the values obtained for VI (1.9 e), VII (1.78 e) and VIII (1.76 e) could be also transferable for an other $[V_{10}O_{28}]^{6-}$ in another environment.

One can notice than the experimental order based on EP estimates (Ob, Oe, Oc, Od, Of and Og) is slightly different to the theoretical one (Ob, Od, Oc, Oe, Og and Of). This is mainly due to the crystal packing which has an influence on the atomic properties. Henry[48] has emphasized, from the PACHA charges, the influence of the partial charges applied to the DV anion.

When looking at the value of the experimental EP projected on the molecular surface in the vicinity of each oxygen atom (Table 7), one can notice that these values are less sensitive (at least independent on the environment of the anion) than the atomic net charges. This remains true for the EP which has been calculated from the net atomic charges. It implies that the EP found experimentally in the solid state is independent of the crystalline environment. Due to the rigidity of the anion, it could be taken as a characterization of the $[V_{10}O_{28}]^{6-}$ transferable to DV anions in other environment. This result will be very useful for the discussion of the interactions of the DV anion with the biological species for instance.

If we compare our experimental characterization of the EP at the molecular surface to those recalculated with the theoretical atomic charges (Mulliken[46] or PACHA charges[48]), one can observe that the Mulliken determination from an *ab initio* SCF calculation give very similar results to those obtained experimentally. This is clear in Figure 7, but also from the EP values reported in Table 7. On the contrary, the PACHA calculation seems not adequate to describe correctly the EP of the DV

anion. Nevertheless, these calculations give the same trend (Ob possesses the most negative EP) according to the linear correlation between the PACHA and the Mulliken charges (Figure 7).

CONCLUDING REMARKS AND FURTHER APPLICATIONS

In this paper, we have characterized the chemical bonds, the net atomic charges and the electrostatic properties of $Na_3[V_{10}O_{28}](C_4N_3OH_5)_3$ $(C_4N_3OH_6)_3 \cdot 10H_2O$ deduced from a high resolution X-ray diffraction experiment. One of the main results is that the EP found at the molecular surface could be considered as "transferable", that means independent of its crystalline environment. Since the DV anion is a rigid entity which remains the same in solution,[33] one can make some hypotheses in order to correlate the properties at the molecular level of the DV anion and its interaction with some biological targets. We will focus on the putative mechanisms of interaction / inhibition / activation and the possible better understanding of those mechanism due to our very precise knowledge of the electronic and electrostatic properties of the DV anion. Therefore we will discuss the biological targets for which a crystallographic structure or electron microscopy with the DV anion as a ligand is known, or with the biological targets for which a docking of DV has been performed.

A large family of ATP-dependent ion pumps, known as P-type ATPases, achieves active transport of cations. The determination of two Ca^{2+}-ATPase structures has been performed by X-ray crystallography.[97,98] Together with cryoelectron microscopy, several conformations have so far been defined. [14,99-101] The papers in the middle of the eighties has demonstrated from biological inhibition of ATPase activity that two binding sites exist for the DV anion.[10,11] The existence of the two sites was confirmed in the 2000 years by Hua et al.[102] All these studies demonstrated that the precise localization of the DV in the different structures of the Ca^{2+}-ATPase could be of great interest for a better understanding of the calcium pump mechanism. Unfortunately the low resolution of the structures concerned has not permitted such a precise determination. Therefore, only new docking modelisation using our experimental EP and hydrogen bond predictions could give new information.

Acid phosphatase A is a respiratory burst-inhibiting acid phosphatase from the American Centers for Disease Control and Prevention (Category A bioterrorism agent) *Francisella tularensis* and prototype of a super-family of acid phosphatases and phospholipases C. Felts et al. [21] has reported the 1.75-Å resolution crystal structure of Acid phosphatase A complexed with the inhibitor orthovanadate, the first published structure for any member of this super-family (**2d1g** code in the Protein Data Bank). The DV anion is linked to the chain B of the asymmetric unit through three histidine and a lysine, to the chain A obtained with a symmetry operation through two asparagine, and to one water molecule. The stronger hydrogen bond interactions between DV and the rest of the protein takes place on the most reactive oxygen atoms (NH…O interactions with a dN…O < 2.70 Å at Ob, Oc, Oe). Therefore, these results show that the hydrogen bond behavior of the DV anion we have observed and described remains the same when the DV anion is bound to a protein.

Tiago et al.[20] have performed a docking study using the structure of truncated *Dictyostelium discoideum* myosin motor domain (**S1dC** code in the Protein Data Bank). These authors have used the theoretical results[46] for the modelisation of the DV assuming that Ob and Oc oxygen atoms have a charge of -2 and the other oxygen atoms have a charge of -1, while the charge of the vanadium atom were fixed to +2.4. We have computed the EP at the molecular surface of the decavanadate anion. The values vary from -6.5 e.Å^{-1} to -9.81 e.Å^{-1} compared to those determined experimentally or theoretically by Kempf et al.[46] (Table 7). The approximation chosen by Tiago et al.,[20] give significant different EP values at the molecular surface, which could imply some uncertainties in the docking results.

Pezza et al.[15] have studied the inhibition of the ATPase activity and the DNA binding capability of bacterial MutS and have shown that the ATPase activity of *Pseudomonas aeruginosa* and *Escheria coli* is inhibited by orthovanadate and DV anion. Docking of DV on the ATP-binding region of MutS showed that energetically more favorable interaction of this compound would take place with the complex MutS-ADP-Mg, suggesting that the inhibitory effect could be produced by a steric impediment of the protein ATP/ADP exchange. New docking, using our precise determination of the electronic and electrostatic properties of the DV anion, could improve these results.

Nilius et al.[103] has tested the effects of the DV on TRPM4 a Ca^{2+}-activated voltage dependent monovalent cation channels, whose activity is potently blocked by intracellular ATP $^{4-}$. The DV induces a dramatic shift in the voltage dependence and decreases the voltage sensitivity of TRPM4 when applied to the inner side of excised patches. Using an analogy approach, the authors have identified the site of DV action resides in the C-terminus of TRPM4. For this case a docking study using our DV properties could give new insight in the understanding of the mechanism.

One can divide the examples explored below in two groups; the first group, constituted by Ca^{2+}ATPase, ABC-ATPase, myosin and TRPM4, contains biological targets against which DV possesses inhibition properties. The second group contains the acid phosphatase A for which the X-DV anion is not supposed to participate to the inhibition. Therefore one can conclude the following: i) Due to the potent different types of interaction (strong and weak DH…O bonds, cations…O), DV could definitively try to be used as a crystallization agent. That could be done in the cases where orthovanadate is an inhibitor. The pH conditions have to be carefully controlled. ii) Our hydrogen bond or cation interaction predictions fit well with the only reported high resolution (**2d1g**) structure. It could even help for determining some remaining water molecules in further structures. iii) Our atomic net charges, hydrogen bond and cation interaction predictions could be suitably used in the docking computations and would probably give better results than the common used charges.

AKNOWLEDGEMENTS.

NB-P, ASdB and UM would thank the French foreign Ministery for a COCOOP support on this project. NB-P and UM would thank the Ministry of Science and Technological Development of the Republic of Serbia (Project 142047). This paper is a part of a join PhD thesis between the University of Belgrade, Faculty of Physical Chemistry and Ecole Centrale Paris. JCP thanks FCT, FEDER, POCI 2010 and PPCDT/QUI/56959/2004.

SUPPORTING INFORMATION.

Tables of atomic coordinates, thermal displacement parameters, bond lengths and bond angles, figures of local coordinates scheme, experimental, dynamic and static deformation maps of different planes are deposited as supporting information. They are available free of charge from the JACS home page (http://pubs.acs.org/JACS).

REFERENCES

(1) Crans, D.C. *Comments Inorg. Chem*. **1994**, *16*, 1.

(2) Aureliano, M.; Crans D.C. *J. Inorg. Biochem.* **2009**, 103, 536.

(3) Chasteen, N.D.; Grady, J.K.; Hoolway, C.E. *Inorg. Chem* **1986**, *25*, 2754.

(4) Soares, S.S.; Aureliano, M.; Joaquim, N.; Coucelo, J.M. *J. Inorg. Biochem.* **2003**, *94*, 285.

(5) Aureliano, M.; Joaquim, N.; Sousa, A.; Martins, H.; Coucelo, J. *J. Inorg. Biochem*. **2002**, *90*, 159.

(6) Farahbakhsh, M.; Schmidt, H.; Rehder, D. *Chem. Ber.* **1997**, *130*, 1123.

(7) Ramos, S.; Tiago, T.; Duarte, R.; Moura, J.J.G.; Aureliano, M. *6th International Vanadium Symposium*, **2008**, 52

(8) Fraqueza, G.; Rito, E.; Brissos, R.; Tiago, T. ;Martins, J.; Duarte, R.O.; Moura, J.J.; Aureliano M. *6th International Vanadium Symposium*, **2008**, 46

(9) Brissos, R.; Fontes, F.L.; Martins, H.; Fraqueza, G.; Tiago, T.; Martins, J.; Duarte, R.O.; Moura, J.G.; Aureliano, M. *6th International Vanadium Symposium*, **2008**, P44

(10) Csermely, P.; Varga, S.; Martonosi, A. *Eur. J. Biochem*. **1985**, *150*, 455.

(11) Csermely, P.; Martonos,i A.; Levy, G.C.; Ejchart, A.J. *Biochem. J.* **1985**, *230*, 807.

(12) Aureliano, M. *J. Inorg. Biochem.* **2000**, *80*, 145.

(13) Krstić, D.; Čolović, M.; Bosnjaković-Pavlović, N.; Spasojević-de Biré, A.; Vasić, V. *Gen. Physiol. Biophys.*, **2009**, in press.

(14) Rice, W.J.; Young, H.S.; Martin, D.W.; Sachs, J.R.; Stokes, D.L. *Biophys. J.* **2001**, *80*, 2187.

(15) Pezza, R.J.; Villarreal, M.A.; Montich, G.G.; Argarana, C.A. *Nucleic Acids Res.* **2002**, 4700.

(16) Aureliano, M. *J. Inorg. Biochem*. **2000**, *80*, 141.

(17) Tiago, T.; Aureliano, M.; Duarte, R.O.; Moura, J.J.G. *Inorg. Chim. Acta* **2002**, 339.

(18) Tiago, T.; Aureliano, M.; Guttierrez-Merino, C.G. *Biochemistry* **2004**, *43*, 5551.

(19) Tiago, T.; Aureliano, M.; Moura, J.J. *J. Inorg. Biochem*. **2004**, *98*, 1902.

(20) Tiago, T.; Martel, P.; Guttierrez-Merino, C.G.; Aureliano, M. *Bioch. Bioph. Acta* **2007**, *1774*, 474.

(21) Felts, R.L.; Reilly, T.J.; Tanner, J.J. *J. Biol.Chem.* **2006**, *281*, 30289.

(22) Boyd, D.W.; Kustin, K.; Niwai, M. *Biochim. Biophys. Acta* **1985**, *827*, 472.

(23) Pluskey, S.; Mahroof-Tahir, M.; Crans, D.C.; Lawrance, D.S. *Biochem J.* **1997**, *321*, 333.

(24) Okamura, N.; Sakai, T.; Nishimura, Y.; Araki, S.; Yamaguchi, M.; Ishibashi, S. *Biol. Pharm. Bull*, **1999**, *22*,799.

(25) Crans, D.C.; Sudkahar, K.; Zamborelli, T.J. *Biochemistry* **1992**, 6812.

(26) Messmore, J.M.; Raines, R.T. *Archive Biochem. Biophys.* **2000**, *381*, 25.

(27) Hir, M. *Biochem. J.* **1991**, *273*, 795.

(28) Soman, G.; Chang, Y.C.; Graves, D.J. *Biochemistry* **1983**, *22*, 4994.

(29) Garcia-Vicente, S. et al. *Diabetes* **2007**, *57*, 486.

(30) Yraola, F.; Garcia-Vicente, S.; Marti, L.; Albericio, F.; Zorzano, A.; Royo, M. *Chem. Biol. Drug Des.* **2007**, *69*, 423.

(31) Aureliano, M.; Gandara, R.M.C. *J. Inorg. Biochem.* **2005**, *99*, 979.

(32) Meicheng, S.; Lifeng, W.; Youqi, T. *Sci. Sin, Ser B* **1984**, *2*, 137.

(33) Crans, D.C. *Comments Inorg. Chem*. **1994**, *16*, 35.

(34) Crans, D.C.; Mahroof-Tahir, M.; Anderson, O.P.; Miller, M.M. *Inorg. Chem*. **1994**, *33*, 5586.

(35) Wang, X.; Liu, H.-X.; You, X.X.;You, X.-Z. *Polyhedron* **1993**, *12*, 77.

(36) Spasojević-de Biré, A.; Kremenović, A.; Morgan, G.; Ghermani, N.E. *J. Phys Chem.* **2002**, *A106,* 12170.

(37) Bouhmaida, N.; Dutheil, M.; Ghermani, N.E.; Becker, P. *J. Chem. Phys.* **2002**, *116*, 14

(38) Ghermani, N.E.; Spasojević-de Biré, A.; Bouhmaida, N.; Ouharzoune, S.; Bouligand, J.; Layre, A.; Gref, R.; Couvreur, P. *Pharm. Res.* **2004**, *21*, 598.

(39) Overgard J.; Hibbs D.E. *Acta Crystallogr*. **2004**, *A60*, 480.

(40) Pizzonero, M.; Keller, L.; Dumas, F.; Ourevitch, M.; Morgan, G.; Ghermani, N. E.; Spasojević-de Biré, A.; Bogdanović, G. A.; d'Angelo, J. *J. Org. Chem*. **2004**, *69*, 4336.

(41) Firley, D.; Courcot, B.; Gillet, J.M.; Fraisse, B.; Zouhiri, F.; Desmaele, D.; D'Angelo, J.; Ghermani, N.E. *J. Phys. Chem.* **2006**, *B110*, 537.

(42) Bergstrom, O.; Gustafsson, T.; Thomas, J.O. *Solid State Ionics* **1998**, *110*, 179.

(43) Claiser, N. DEA report, Université Henri Poincaré, Nancy, **2000**

(44) Ozerov, R.P.; Streltsov, V.A.; Sobolev, A.N.; Figgis, B.N.; Volkov, V.L. *Acta Crystallogr*. **2001**, *B57*, 244.

(45) Rohmer, M.M.; Ernenwein, R.; Ulmschneider, M.; Wiest, R.; Benard, M. *Int. J. Quantum Chem.* **1991**, *40*, 723.

(46) Kempf, J.Y.; Rohmer, M.M.; Poblet, J.M.; Bo, C.; Benard, M. *J. Am. Chem. Soc*. **1992**, *114*, 1136.

(47) Rohmer, M.M.; Benard, M.; Blaudeau, J.P.; Maestre, J.M.; Poblet, J.M. *Coord. Chem. Rev.* **1998**, *178-180*, 1019

(48) Henry, M. *J. Cluster Sci.* **2002**, *13*, 437

(49) Brown, I.D.; Shannon, R.D. *Acta Cryst.* **1973**, *A29*, 266.

(50) Klemperer, W.G.; Shum, W. *J. Am. Chem. Soc.* **1977**, *99*, 3544.

(51) Bogdanović, G.A.; Bošnjaković-Pavlović, N.; Spasojević-de Biré, A.; Ghermani, N.E.; Mioč, U. *J. Serb. Chem. Soc.* **2007**, *72*, 545.

(52) Hansen, N.; Coppens, P. *Acta Crystallogr.* **1978**, *A34*, 909.

(53) Coppens, P. in *X-ray charge densities and chemical bonding.* Oxford: International Union of Crystallography/Oxford University Press, 1997.

(54) Coppens, P.; Guru Row, T.N.; Leung, P.; Stevens, E.D.; Becker, P.;Yang, Y.W. *Acta Crystallogr*. **1979**, *A35*, 63.

(55) Bader, R.F. in *Atoms in molecules: A Quantum Theory* Int. Series of Monographs in Chemistry 22, Oxford University Press: Oxford, 1990.

(56) Cremer, D.; Kraka, E. *Angew. Chem., Int. Ed. Engl.* **1984**, *23*, 627.

(57) Cremer, D.; Kraka, E. *Croat. Chem. Acta* 1**984**, *57*, 1259.

(58) Abramov, Y.A. *Acta Crystallogr*. **1997,** *A53*, 264.

(59) Souhassou, M.; Blessing, B. *J. Appl. Crystallogr*. **1999**, *32*, 210.

(60) Souhassou, M. *19th European Crystallographic Meeting*, **2000**, 195

(61) Holladay, A.**;** Leung, P.; Coppens, P. *Acta Crystallogr*. **1983**, *A39*, 377.

(62) Ghermani, N.E.; Bouhmaida, N.; Lecomte, C. *Internal report UMR CNRS 7036, Université Henri Poincaré, Nancy1, France and UMR CNRS 8612, Université Paris XI, France*, **1992-2001**

(63) Drechsel, E. *Ber.* **1887**, *20*, 1452.

(64) Chinea, E.; Dakternieks, D.; Duthie, A.; Ghilardi, C.A.; Gili, P.; Mederos, A.; Midollini, S.; Orlandini, A. *Inorg. Chim. Acta* **2000**, *298*, 172.

(65) Bruker-AXS, *Analytical X-ray Instruments Inc., Madison* **1998**.

(66) Blessing, R.H. *J. Appl. Crystallogr*. **1997**, *30*, 421.

(67) Altomare, A.; Cascarano, G.; Giacovazzo, C.; Guagliardi, A.; Burla, M.C.; Polidori, G.; Camalli, M. *J. Appl. Crystallogr.* **1994,** *27*, 435.

(68) Sheldrick, G.M. *University of Göettingen, Germany,* **1997**.

(69) Farrugia, L.J. *Appl. Cryst.* **1999**, *32*, 837.

(70) Burnett, M.N.; Johnson, C.K. *Oak Ridge National Laboratory, Tenessee, USA* **1996**.

(71) Coppens, P. *Coord. Chem. Rev.* **1985**, *65*, 285.

(72) International Tables for X-ray Crystallography; Kynoch Press: Birmingham, U.K. **1974**, IV pp 103.

(73) Macchi, P.; Garlaschelli, L.; Martinengo, S.; Sironi, A. *J. Am. Chem. Soc*. **1999**, *121*, 10428.

(74) Ozerov, R.P.; Streltsov, V.A.; Sobolev, A.N.; Figgis, B.N.; Volkov, V.L. *Acta Crystallogr*. **2001**, *B57*, 244.

(75) Farrugia, L.J.; Mallinson, P.R.; Stewart, B. *Acta Crystallogr.* **2003**, *B59*, 234.

(76) Martin, M.; Rees, B.; Mitschler, A. *Acta Crystallogr*. **1982**, *B38*, 6.

(77) Rees, B. *Acta Crystallogr*. **1976**, *A32*, 483.

(78) See crystal structure studies references in Table S1, Supplementary Information Material.

(79) Allen, F.H. *Acta Crystallogr*. **2002**, *B58*, 380.

(80) See crystal structure studies references in Table S2, Supplementary Information Material.

(81) ICSD, *Fachinformationszentrum (FIZ) Karlsruhe* **2007**.

(82) See crystal structure studies references in Table S3, Supplementary Information Material.

(83) See crystal structure studies references in Table S4, Supplementary Information Material.

(84) Kruger, T.; Bruhn, C.; Steinborn, D. *Org. Biomol. Chem*. **2004**, *2*, 2513.

(85) Muller, J.; Freisinger, E. *Acta Crystallogr.* **2005**, *E61*, o320.

(86) Muller-Dethlefs, K.; Hobza, P. *Chem. Rev*. **2000**, *100*, 143.

(87) See crystal structure studies references in Table S5, Supplementary Information Material.

(88) Bader, R.F.; Preston, H.J.T. *Int. J. Quantum Chem* **1969**, *3*, 327.

(89) Espinosa, E.; Molins, E.; Lecomte, C. *Chem. Phys. Lett.* **1998**, *285*, 170.

(90) Espinosa, E.; Souhassou, M.; Lachekar, H.; Lecomte, C, *Acta Crystallogr.* **1999**, *B55*, 563

(91) Desiraju, G.R.; Steiner, T. in *The Weak Hydrogen Bond in Structural Chemistry and Biology.* Oxford Univ. Press, Oxford, 1999

(92) Kubicki, M.; Borowiak, T.; Dutkiewicz, G.; Souhassou, M.; Jelsch, C.; Lecomte, C. *J. Phys. Chem* **2002**, *B106,* 3706.

(93) Spasojević-de Biré, A.; Nguyen, Q.D.; Becker, P.J.; Benard, M.; Strich, A.; Thieffry, C.; Hansen, N.K.; Lecomte, C. in *Application of charge density research to chemistry and drug design.* NATO Asi Series, Jeffrey Ed., Plenum Publisher, New York **1991**, pp 385.

(94) Spasojević-de Biré, A.; Dao, N.Q.; Hansen, N.K.; Fisher, E.O. *Inorg. Chem.* **1993**, *32*, 5354.

(95) Lee, C.R.; Wang, C.C.; Chen, K.C.; Lee, G.H.; Wang, Y. *J. Phys. Chem.* **1999**, *A103*, 156.

(96) Volkov, A.; Gatti, C.; Abramov, Y.; Coppens, P. *Acta Crystallogr.* **2000**, *A56*, 252.

(97) Toyoshima, C.; Nakasako, M.; Nomura, H.; Ogawa H. *Nature.* **2000**, *405*, 647.

(98) Toyoshima, C.; Nomura, H. *Nature* **2002**, *418*, 605.

(99) Stokes, D.L.; Green, N.M. *Biophys. J.* **2000**, *78*, 1765.

(100) Xu, C.; Rice, W.J.; He, W.; Stockes, D.L. *J. Mol. Biol.* **2002**, *316*, 201.

(101) Hinsen, K.; Reuter, N.; Navaza, J.; Stokes, D.L.; Lacapere, J.J. *Biophys. J.* **2005**, *88*, 818.

(102) Hua, S.; Inesi, G. *J. Biol. Chem.* **2000**, *275*, 30546.

(103) Nilius, B.; Prenen, J.; Janssens, A.; Voets, T.; Droogmans, G. *J. Physiol.* **2004**, *560*, 753.

TABLE CAPTIONS

Table 1. X-ray diffraction experiment and refinement details [a]

[a] The value R_{int}, gof, R_1 and wR_1 are defined as $R_{int} = \sum_H \left[\frac{N_H}{N_H - 1}\right]^{\frac{1}{2}} \sum_{i=1}^{N_H} \left|I_i(H) - I_i^{mean}(H)\right| / \sum_H \sum_{i=1}^{N_H} \left|I_i(H)\right|$ I(H) is the observed reflection intensity for H vector. N(H) is the number of equivalent and redundant reflections. $R = \sum \left\|F_{obs}\right| - \left|F_{calc}\right\| / \sum \left|F_{obs}\right|$, $R_w = \left[\sum w(F_{obs} - F_{calc})^2 / \sum wF_{obs}^2\right]^{\frac{1}{2}}$, $GOF = \left[\sum w\left[F_{obs}^2 - F_{calc}^2\right]^2 / (m_{obs} - n_p)\right]^{\frac{1}{2}}$. The statistical weight is $w = 1/\sigma^2(F_{obs})$ or $1/\sigma^2(F_{obs}^2)$ where σ^2 is the variance, m_{obs} and n_p are the number of observations and refined parameters, respectively.

Table 2. Intramolecular distances and topology analysis of the DV anion [b]

[b] Different V-O distances (Å) are reported according to the vanadium and oxygen classification. This work (estimated standard deviations in parentheses), theoretical data from Kempf [48] and average values from 37 structures retrieved in CSD bases (second column in italic). Results of the topological analysis of charge density at (3,-1) (BCP) of the DV anion. Our results ($\rho(r_{cp})$ is the electron density at the BCP ($eÅ^{-3}$), $\nabla^2\rho(r_{cp})$ is Laplacian at the BCP ($eÅ^{-5}$), ε is ellipticity, λ_1, λ_2, λ_3 are the eigenvalues at the BCP, H is the total energy density ($Kcal.mol^{-1}$) are compared to the $\rho(r_{cp})$ and $\nabla^2\rho(r_{cp})$ theoretical data.[45]

Table 3. Selected bond lengths (Å) in cytosine molecules with estimated standard deviations in parentheses

Table 4. Distances (Å) and angles (°) of the hydrogen bonds (D donor, A acceptor) [c]

[c] Estimated standard deviations are given in parentheses. (i) = -x,-y+1,-z+2, (ii) = -x+1,-y+1,-z+2, (iii) = x,+y,+z+1, (iv) = -x+2,-y,-z+1, (v)= x+1,+y,+z, (vi) = -x+1,-y,-z+2, (vii)= -x+1,-y+1,-z+1, (viii) = +x,+y,+z-1, (ix) = x-1,+y,+z, (x) = -x,-y+1,-z+1. Results of the topology analysis are given. Unit are given in Table 2. d_1 and d_2 are BCP-atoms distance (Å).

Table 5. Experimental determination of the *d* orbital (e) populations of the vanadium in the DV anion

Table 6. Experimental and theoretical net atomic charge (e) for vanadium atoms in a DV anion

Table 7. Experimental and theoretical net atomic charges (e) and EP ($eÅ^{-1}$) at the molecular surface in the vicinity of the oxygen atoms of the DV anion

FIGURE CAPTIONS

Figure 1. ORTEP views of the Na_3 $[V_{10}O_{28}]$ $(C_4N_3OH_5)_3(C_4N_3OH_6)_3$. $10H_2O$ structure. a) and b) labeling scheme and type of atoms for the SV anion, c) cytosine - cytosinium interactions between cytosinium A and A'and d) octahedral environment of sodium atoms.

Figure 2. Residual electron density maps. a) DV-horizontal plane (plane containing O10, O11, O21, O27, O22, O61, V3, V4 and V5 atoms), b) DV-vertical-XZ plane (plane containing O12, O13, O22, O61, V1 and V2 atoms) c) DV-vertical-YZ (plane containing O31 O32 and V4 atoms). O61 oxygen atoms are omitted. Contour intervals are 0.1 $eÅ^{-3}$. Negative contours are dashed.

Figure 3. Crystal packing. The DV – sodium chains. Cytosine molecules have been omitted.

Figure 4. Static model deformation density. Planes a) and b) and contours as defined in Figure 2. c) DV-vertical-YZ (plane containing O31 O32 and V4 atoms). The longest V-O bonds (VI-Oa, VII-Oa, VIII-Oa) in the cage are in yellow, the medium bonds are in green (VII-Od) and blue (VII-Oe) color and shortest V-O bonds (VI-Oe, VIII-Of, VII-Og) are in red color. The other bonds are in dark color.

Figure 5. Behavior of $\rho(r_{cp})$ of the V-O bond as a function of the interatomic distance.

Figure 6. Static deformation density of D-H…A hydrogen bonds. Planes containing a)O32, H1w′ and O1w, b)O25, $H4c^{(viii)}$ and $H5w^{(vii)}$, c)O24, $H4c^{(viii)}$ and $H4b^{(viii)}$, d) O22, $H4c^{(viii)}$ and $H5c^{(viii)}$, e) O10, $H5a^{(i)}$ and $H5b^{(vi)}$, f) Na2, O5w and Na1 atoms. Contours as defined in Figure 2.

Figure 7. Experimental EP on the molecular surface (0.007 $e.Å^{-3}$) (column 1-4). Column 1-3 Na_3 $[V_{10}O_{28}]$ $(C_4N_3OH_5)_3$ $(C_4N_3OH_6)_3 \cdot 10H_2O$, colomn 4 $(NH_4)_6$ $[V_{10}O_{28}]$. $6H_2O$. Electrostatic potential of the decavanadate isolated from the crystal computed from the multipole refinement (column 1), from the charge determined by the AIM method (column 2), and by a κ refinement (column 3 and

4). Theoretical EP (column 5-6) computed from the charge determined by the Mulliken partitioning (collumn 5) and by a PACHA partitioning (column 6).

Table 1.

Chemical formula	$Na_3[V_{10}O_{28}](C_4N_3OH_5)_3\ (C_4N_3OH_6)_3 \cdot 10H_2O$
Temperature (K)	210(1)
Wavelength (Å)	0.71073
Cell setting, space group	triclinic, $P\bar{1}$
Z	1
Crystal size: (mm) x (mm) x (mm)	0.36 x 0.29 x 0.18
Density (calculated) (Mg/m^3)	2.12
a (Å)	9.8526(1)
b (Å)	12.2227(1)
c (Å)	13.0852(1)
α (°)	85.995(1)
β (°)	80.110(1)
γ (°)	70.954(1)
Volume($Å^3$)	1467.25(3)
$[\sin\theta/\lambda]_{max}$ ($Å^{-1}$)	1.11
Scan width (°) / scan method	0.15° / Δω scan
Crystal-to-detector distance (d) (cm)	4.075
Total frames / time per frame (s)	38400 /2 to 30
Absorption correction	SADABS
Total measured reflexions	221 309
$R_{int}(F^2)$ before SADABS	0.071
$R_{int}(F^2)$ after SADABS	0.031
Number of reflexions used after SADABS	207 128
R_{int}	0.0276
Number of reflexions used in SHELX : all data / unique ($F_0 > 4\sigma F_0$)	28 757 / 20 587
Spherical refinement : R(%) / R_w(%) / GOF / parameters	2.88 / 3.27 / 1.28 / 28
Number of reflexions used in MOLLY($I>3\sigma(I)$)	18 394
κ refinement : R (%) / R_w (%) / GOF / parameters	2.76 / 2.97 / 1.16 / 20
Multipole refinement : R (%) / R_w (%) / GOF / parameters	2.32 / 2.34 / 0.91 / 505

Table 2.

Vanadium atoms	Type of Vanadium bonds	bond	distance		ρ_{cp}		$\nabla^2\rho(r_{cp})$		ε	λ_1	λ_2	λ_3	$H(r_{cp})$
			this work	Kempf[46]	this work	Kempf[46]	this work	Kempf[46]					
V-Oa	**VI-Oa** *2.113*	V4-O61	2.0781(5)	2.116	0.52	0.47	8.87	7.59	0.01	-2.09	-2.08	13.04	-5.71
		V4-O61	2.1583(5)		0.44		6.90		0.05	-1.63	-1.56	10.09	-3.84
	VII-Oa *2.323*	V3-O61	2.3324(5)	2.316	0.32	0.28	4.36	5.52	0.03	-0.94	-0.91	6.2	-1.98
		V5-O61	2.2937(5)		0.34		4.72		0.10	-1.02	-0.93	6.68	-2.22
	VIII-Oa *2.244*	V1-O61	2.2679(6)	2.243	0.37	0.34	5.17	6.49	0.013	-1.19	-1.18	7.54	-1.94
		V2-O61	2.2414(5)		0.37		5.34		0.06	-1.13	-1.06	7.52	-2.40
V-Ob	**VI-Ob** *1.928*	V4-O31	1.9217(5)	1.927	0.77	0.77	13.66	9.59	0.03	-4.1	-3.98	21.72	-18.09
		V4-O32	1.9427(5)		0.74		12.76		0.03	-3.94	-3.82	20.52	-17.09
	VIII-Ob *2.006*	V1-O32	1.9981(6)		0.65		11.04		0.03	-3.25	-3.14	17.43	-12.77
		V1-O31	2.0205(5)	2.013	0.58	0.62	10.04	8.60	0.03	-2.60	-2.52	15.16	-8.37
		V2-O31	2.0040(5)		0.65		10.95		0.03	-3.25	-3.17	17.36	-12.70
		V2-O32	2.0268(6)		0.58		10.02		0.13	-2.76	-2.43	15.21	-8.77
V-Oc	**VII-Oc** *1.880*	V3-O20	1.8504(6)		0.79		14.49		0.03	-4.1	-3.96	22.55	-18.83
		V3-O25	1.8716(5)	1.883	0.85	0.84	14.99	10.63	0.06	-4.91	-4.64	24.54	-24.63
		V5-O23	1.8795(5)		0.86		14.83		0.04	-4.91	-4.72	24.46	-26.38
		V5-O24	1.8911(5)		0.86		14.61		0.07	-5.1	-4.72	24.47	-26.97
	VIII-Oc *1.821*	V1-O23	1.8132(6)		1.06		17.77		0.05	-6.88	-6.54	31.19	-44.12
		V1-O20	1.8338(6)	1.826	0.97	0.97	17.45	12.41	0.04	-5.83	-5.59	28.87	-32.89
		V2-O24	1.8141(6)		1.05		17.55		0.02	-6.55	-6.45	30.54	-42.70
		V2-O25	1.8240(6)		1.00		17.70		0.04	-6.07	-5.82	29.54	-36.40
V-Od	**VII-Od** *1.832*	V3-O22	1.8871(6)	1.831	0.94	0.95	16.00	12.19	0.11	-5.76	-5.2	26.96	-32.90
		V5-O22	1.8795(6)		1.03		16.58		0.09	-6.65	-6.12	29.35	-42.65
V-Oe	**VI-Oe** *1.688*	V4-O27	1.6848(5)	1.697	1.42	1.35	24.62	17.42	0.04	-9.55	-9.21	43.39	-80.50
		V4-O21	1.7059(6)		1.29		24.66		0.04	-8.30	-7.98	40.94	-60.71
	VII-Oe *2.049*	V3-O21	2.0183(6)	2.032	0.57	0.55	9.88	8.46	0.08	-2.64	-2.43	14.95	-7.80
		V5-O27	2.0697(6)		0.54		8.78		0.05	-2.49	-2.38	13.75	-7.45
V-Of	**VIII-Of** *1.609*	V1-O13	1.6189(6)	1.614	1.79	1.66	29.10	22.48	0.04	-13.67	-13.18	55.96	-133.72
		V2-O12	1.6230(6)		1.61		28.85		0.09	-11.74	-10.76	51.36	-102.93
V-Og	**VII-Og** *1.603*	V3-O11	1.6115(6)	1.605	1.71	1.68	30.96	22.32	0.06	-12.28	-11.54	54.78	-114.57
		V5-O10	1.6120(6)		1.75		30.17		0.11	-13.54	-12.24	55.95	-124.92

Table3.

bond	Cytosinium A	Cytosinium B	Cytosine C
C4-N4	1.325(1)	1.322(1)	1.317(1)
C4-C5	1.430(1)	1.428(1)	1.427(11)
C5-C6	1.360(1)	1.359(1)	1.351(2)
C6-N1	1.357(1)	1.358(1)	1.385(2)
N1-C2	1.372(1)	1.363(1)	1.362(2)
C2-N3	1.372(1)	1.365(1)	1.357(1)
N3-C4	1.351(1)	1.354(1)	1.351(1)
C2-O2	1.242(1)	1.240(1)	1.254(2)

Table 4.

	D-H ···A	d (H-A)	d(D··A)	∠DHA	d_1	d_2	$\rho(r_{cp})$	$\nabla^2\rho(r_{cp})$	ε	λ_1	λ_2	λ_3	$H(r_{cp})$
O-H…O													
	O1w-H1w'···O32	1.6924(5)	2.6535(8)	174.49(5)	1.692	0.533	0.20	6.39	0.04	-0.95	-0.91	8.25	8.78
	O2w-H2w'···O20$^{(v)}$	1.7049(6)	2.672(1)	176.92(6)	1.705	0.547	0.18	5.96	0.02	-0.83	-0.82	7.60	8.72
	O4w-H4w'···O31$^{(x)}$	1.7583(5)	2.7201(9)	177.40(5)	1.758	0.570	0.15	5.30	0.02	-0.62	-0.61	6.53	8.28
	O2w-H2w ···O21	1.8311(5)	2.753(1)	159.29(6)	1.831	0.668	0.14	3.49	0.30	-0.75	-0.57	4.82	4.62
	O5w-H5w'···O2b	1.8439(7)	2.777(1)	162.16(5)	1.844	0.662	0.11	3.51	0.31	-0.66	-0.5	4.67	5.54
	O3w-H3w'···O12$^{(x)}$	1.8620(6)	2.8132(9)	169.01(5)	1.862	0.654	0.10	3.58	0.29	-0.53	-0.42	4.53	6.03
	O5w-H5w···O25$^{(vii)}$	1.8921(6)	2.8356(9)	164.95(5)	1.892	0.647	0.09	3.62	0.22	-0.37	-0.30	4.29	6.46
	O3w-H3w···O2c$^{(ix)}$	1.9730(9)	2.841(1)	148.40(6)	1.973	0.769	0.10	2.31	0.33	-0.53	-0.4	3.23	3.39
	O2w-H2w′···O11$^{(iv)}$	2.8023(7)	3.306(1)	113.23(5)									
	O4w-H4w···O11$^{(vii)}$	2.8271(7)	3.315(1)	112.60(5)									
	O1w-H1w′···O12	2.9091(7)	3.449(1)	115.72(5)									
	O2w-H2w···O11$^{(iv)}$	2.9382(7)	3.306(1)	103.95(5)									
	O5w-H5w···O12$^{(vii)}$	2.9378(7)	3.302(1)	103.67(5)									
	O3w-H3w′···O13$^{(x)}$	2.9904(6)	3.3954(9)	106.75(4)									
N-H…O	**D-H ···A**												
	N1a-H1a··O4w	1.7006(7)	2.705(1)	173.70(6)	1.701	0.531	0.19	6.26	0.04	-0.96	-0.92	8.14	9.03
	N4c-H3c···O2b$^{(ii)}$	1.7475(8)	2.756(1)	173.49(6)	1.748	0.595	0.27	3.74	0.02	-1.56	-1.53	6.84	-0.35
	N1b-H1b···O1w	1.7519(7)	2.757(1)	173.48(6)	1.752	0.597	0.17	4.32	0.26	-0.99	-0.79	6.1	5.52
	N4a-H3a···O2a$^{(i)}$	1.8324(7)	2.841(1)	177.12(6)	1.834	0.641	0.20	3.01	0.03	-1.11	-1.08	5.21	1.40
	N4b-H4b···O24$^{(viii)}$	1.8536(5)	2.8603(9)	174.92(5)	1.854	0.632	0.09	3.77	0.52	-0.46	-0.3	4.53	6.78

	N4b-H3b···O2c$^{(ii)}$	1.866(1)	2.874(2)	178.47(7)	1.866	0.619	0.09	3.86	0.38	-0.42	-0.31	4.59	7.06
	N4a - H4a···O23$^{(i)}$	1.8678(6)	2.8581(9)	166.44(6)	1.867	0.707	0.12	2.80	0.66	-0.77	-0.47	4.04	3.86
	N4c-H4c···O22$^{(iii)}$	1.8798(5)	2.875(1)	169.84(1)	1.879	0.695	0.13	2.53	0.49	-0.66	-0.45	3.64	3.06
	N1c-H1c···O2w	2.288(1)	3.084(2)	155.6(1)									
	N1c-H1c···O20$^{(v)}$	2.4963(5)	3.1466(6)	135.8(1)									
	N4c-H4c···O25$^{(viii)}$	2.7832(6)	3.373(1)	117.91(6)									
	N4c-H4c···O24$^{(viii)}$	2.9210(6)	3.407(1)	110.55(6)									
N-H…N	**D-H ···A**												
	N3b-H2b···N3c$^{(ii)}$	1.8087(9)	2.816(1)	173.39(5)	1.801	0.594	0.39	1.78	0.03	-2.3	-2.22	6.31	-11.72
	N3a-H2a···N3a$^{(i)}$	1.8491(8)	2.838(2)	167.72(2)									
C-H…O	**D-H ···A**												
	C5b-H5b···O10$^{(vi)}$	2.0702(6)	3.150(1)	98.22(6)									
	C5a-H5a···O10$^{(i)}$	2.2430(7)	3.304(1)	165.93(6)	2.242	0.865	0.04	1.25	0.60	-0.16	-0.1	1.52	2.28
	C6c-H6c···O11$^{(iv)}$	2.4177(8)	3.222(2)	144.9(1)	2.417	1.016	0.08	0.95	0.08	-0.24	-0.22	1.42	0.84
	C6b-H6b···O10	2.6784(7)	3.292(1)	115.46(6)									
	C5c-H5c···O22$^{(iii)}$	2.6819(5)	3.489(1)	130.78(6)									
	C6b-H6b···O23	2.7570(6)	3.147(1)	100.89(6)	2.758	1.281	0.06	0.70	0.29	-0.16	-0.13	0.99	0.75
	C6a-H6a···O11$^{(vii)}$	2.8154(7)	3.384(1)	112.86(6)									
	C6c-H6c···O22$^{(iv)}$	2.8392(5)	3.390(1)	119.2(1)									

Table 5.

	V(I)	V(II)	V(III)
d_{z2}	0.57(4)	0.70(5)	0.68(5)
d_{x2-y2}	0.68(4)	0.61(5)	0.68(5)
d_{xy}	0.60(8)	0.60(9)	0.61(8)
d_{xz}	0.62(4)	0.66(5)	0.57(5)
d_{yz}	0.56(4)	0.64(5)	0.67(5)
d orbital population	3.03(5)	3.20(5)	3.20(5)

Table 6.

		Experimental				Theoretical	
		$Na_3[V_{10}O_{28}](C_4N_3OH_5)_3(C_4N_3OH_6)_3 \cdot 10H_2O$ This work			$(NH_4)_6V_{10}O_{28}.6H_2O$ Bogdanovic et al.[51]	$[V_{10}O_{28}]^{6-}$ Henry[48]	$[V_{10}O_{28}]^{6-}$ Kempf et al.[46]
atom	**type**	**Multipole refinement**	**AIM**	**κ refinement**	**κ refinement**	**PACHA**	**Mulliken**
V4	**I**	+1.97(5)	+1.688	+1.94(5)	+2.0(1) +1.9(1)	+1.514	+2.13
V3	**II**	+1.79(5)	+1.540	+1.85(5)	+1.7(1) +1.8(1)	+1.865	+2.04
V5		+1.81(5)	+1.509	+1.71(5)	+1.6(1) +1.6(1)	+1.870	
V1	**III**	+1.80(5)	+1.533	+1.74(5)	+1.6(1) +1.6(1)	+1.780	+2.05
V2		+1.80(5)	+1.535	+1.78(5)	+1.7(1) +1.6(1)	+1.766	

Table 7.

		Experimental							Theoretical			
		$Na_3[V_{10}O_{28}](C_4N_3OH_5)_3(C_4N_3OH_6)_3 \cdot 10H_2O$ This work					$(NH_4)_6V_{10}O_{28} \cdot 6H_2O$ Bogdanovic et al.[51]		$[V_{10}O_{28}]^{6-}$ Henry[48]		$[V_{10}O_{28}]^{6-}$ Kempf et al.[46]	
		Multipole refinement	κ refinement		AIM		κ refinement		PACHA		Mulliken	Ab initio SCF
		EP	charge	EP	charge	EP	charge	EP	charge	EP	charge	EP
O61	a		-0.88(5)		-0.724		-0.7(1)		-0.861		-1.27	
O31 O32	b	-8.7	-0.97(5) -1.08(5)	-8.2	-0.873 -0.918	-8.7	-0.9(1) -0.6(1)	-8.5	-0.726 -0.713	-7.4	-1.04	-8.2
O24 O25 O20 O23	c	-7.2	-0.90(5) -0.84(5) -0.81(5) -0.91(5)	-6.9	-0.857 -0.799 -0.808 -0.900	-7.1	-1.2(1) -0.6(1) -1.0(1) -0.7(1)	-7.1	-0.666	-6.1	-0.93	-6.8
O22	d	-6.9	-0.93(5)	-6.6	-0.797	-6.8	-1.0(1)	-6.9	-0.686	-5.8	-0.94	-6.5
O21 O27	e	-7.4	-0.87(5) -0.92(5)	-7.1	-0.783 -0.733	-7.4	-0.8(1) -0.5(1)	-7.2	-0.635	-6.4	-0.82	-7.0
O13 O12	f	-6.2	-0.63(5) -0.81(5)	-5.9	-0.573 -0.668	-6.2	-1.1(1) -0.7(1)	-6.4	-0.555	-5.3	-0.63	-5.9
O11 O10	g	-5.8	-0.84(5) -0.65(5)	-5.6	-0.717 -0.620	-5.8	-0.5(1) -1.2(1)	-5.7	-0.560	-4.9	-0.66	-5.5

Figure 1.

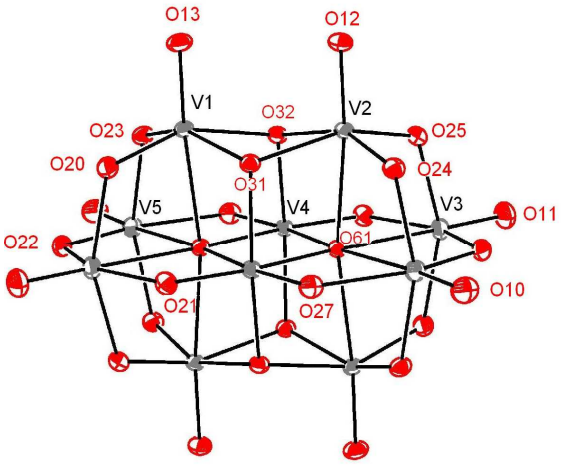

a)

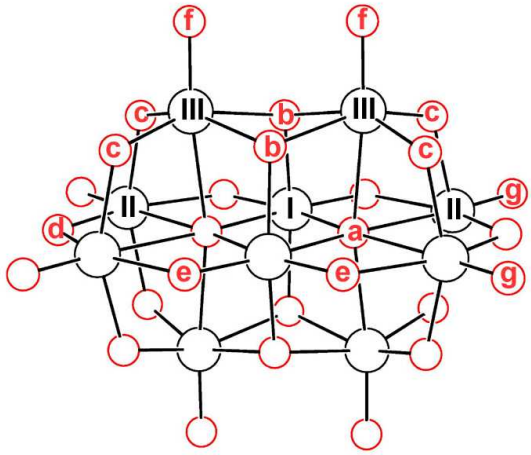

b)

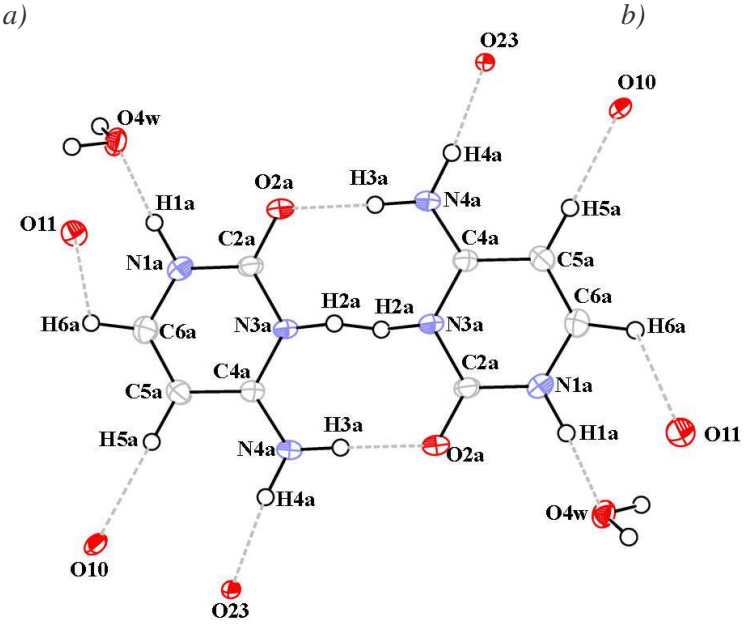

c)

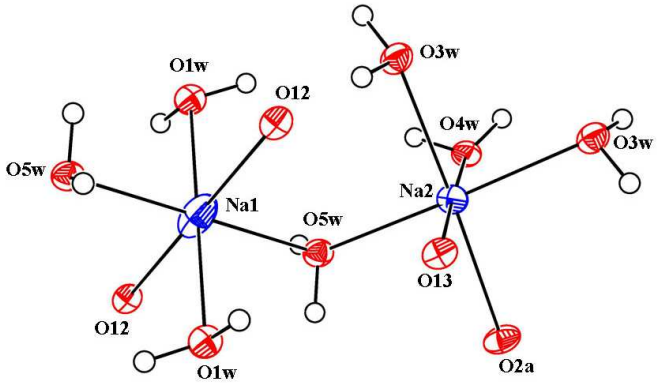

d)

Figure 2

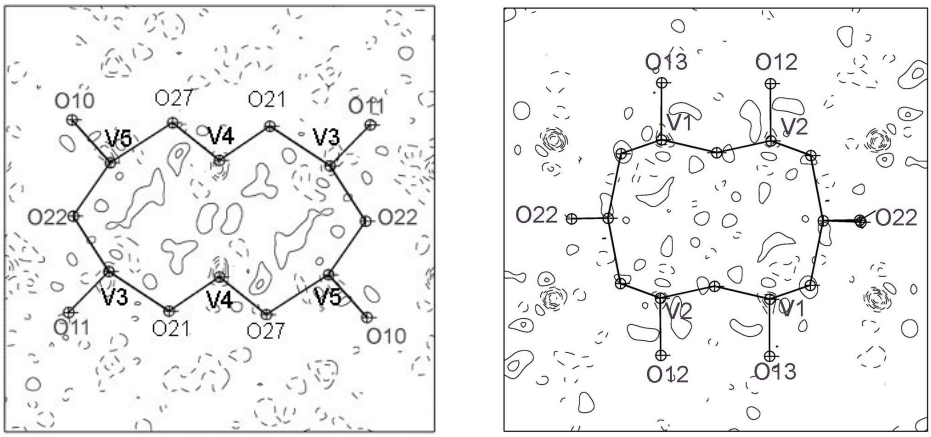
O10
O27
O21
O11
V5
V4
V3
O22
O22
V3
V4
V5
O11
O21
O27
O10
O13
O12
V1
V2
O22
O22
V2
V1
O12
O13

a) b)

Figure 3.

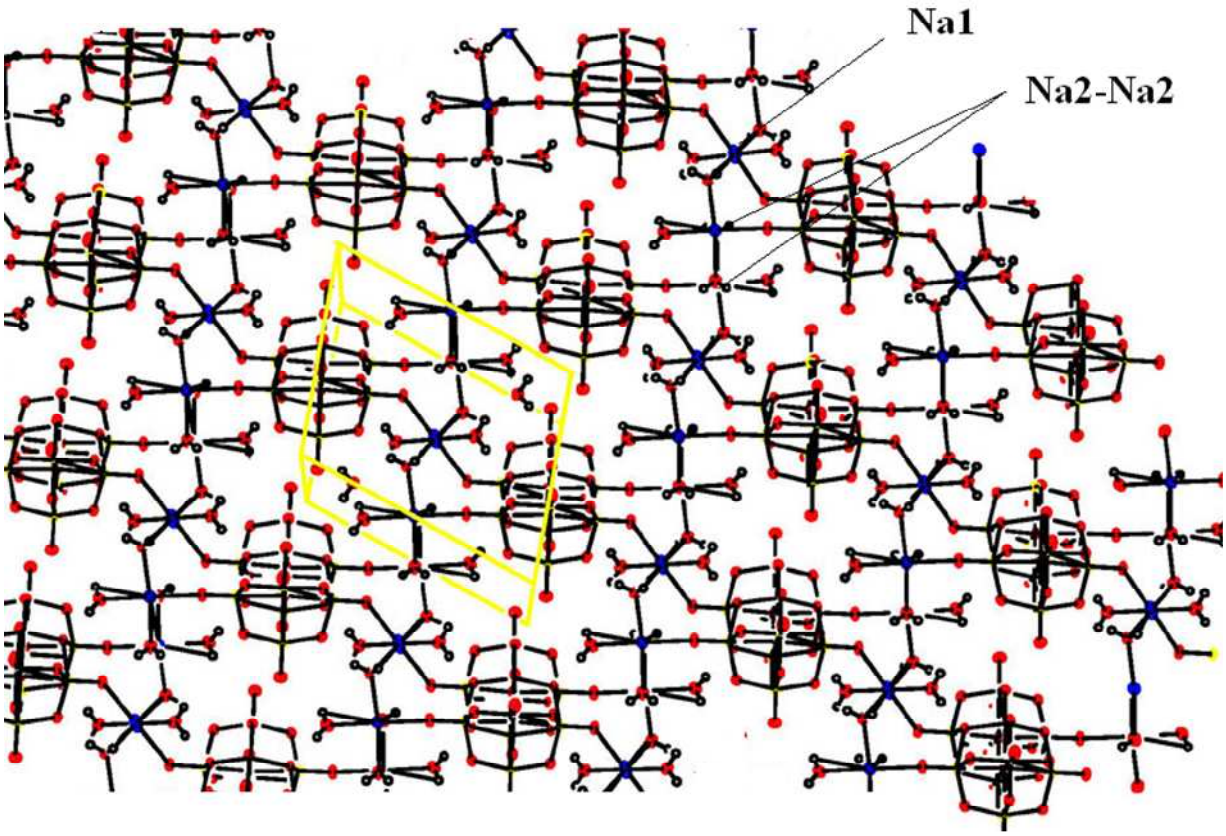

Figure 4.

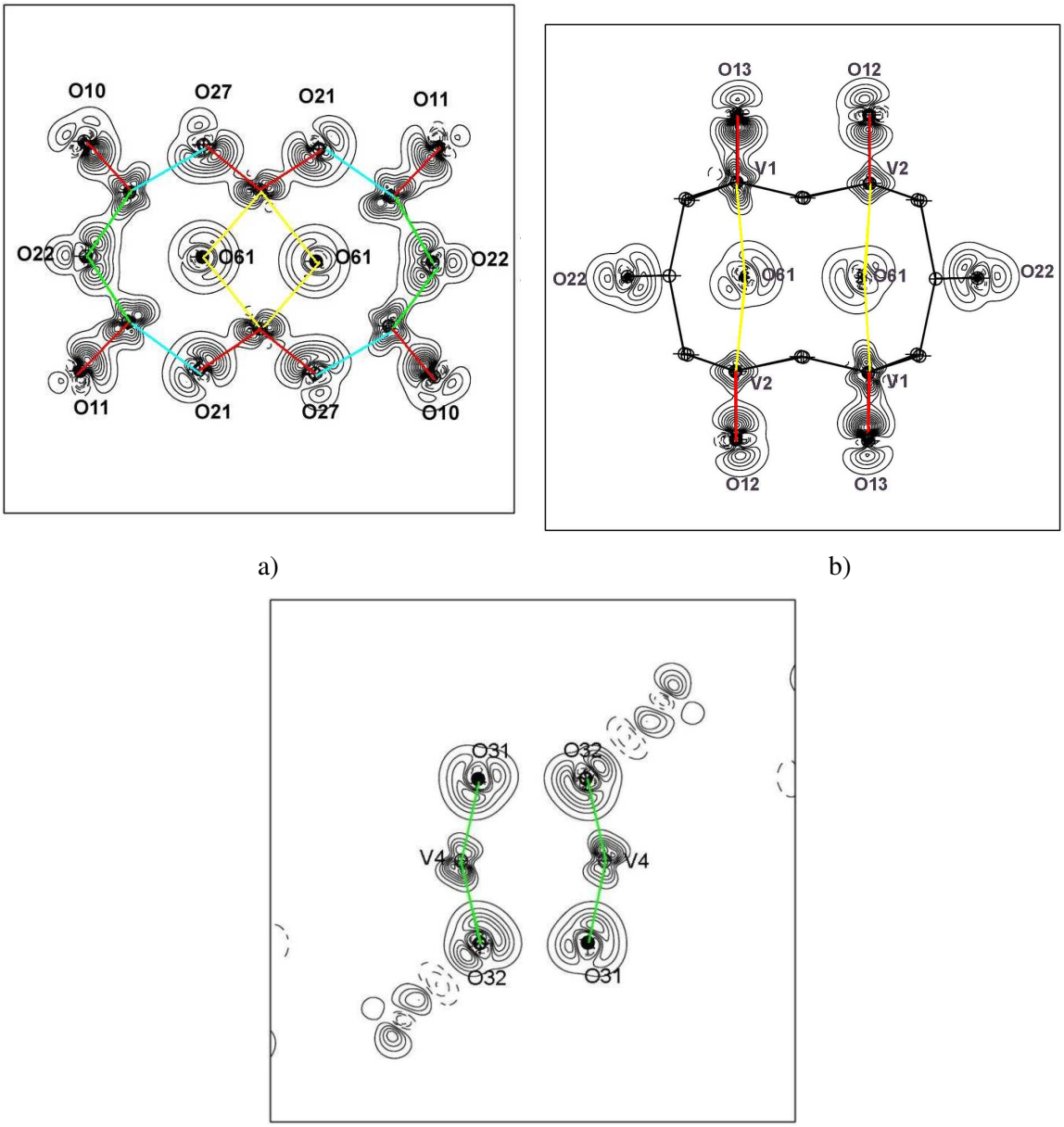
O10
O27
O21
O11
O22
O61
O61
O22
O11
O21
O27
O10
a)
O13
O12
V1
V2
O22
O61
O61
O22
V2
V1
O12
O13
b)
O31
O32
V4
V4
O32
O31
c)

Figure 5.

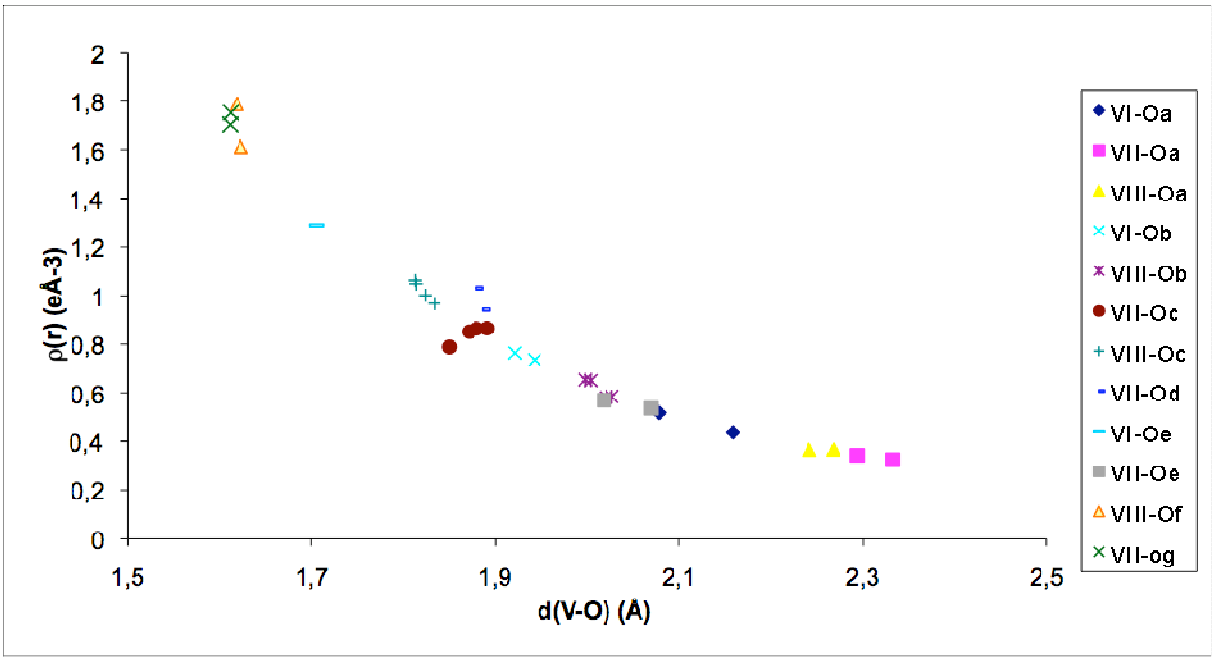
ρ(r) (eÅ-3)
d(V-O) (Å)
2
1,8
1,6
1,4
1,2
1
0,8
0,6
0,4
0,2
0
1,5
1,7
1,9
2,1
2,3
2,5
VI-Oa
VII-Oa
VIII-Oa
VI-Ob
VIII-Ob
VII-Oc
VIII-Oc
VII-Od
VI-Oe
VII-Oe
VIII-Of
VII-og

Figure 6.

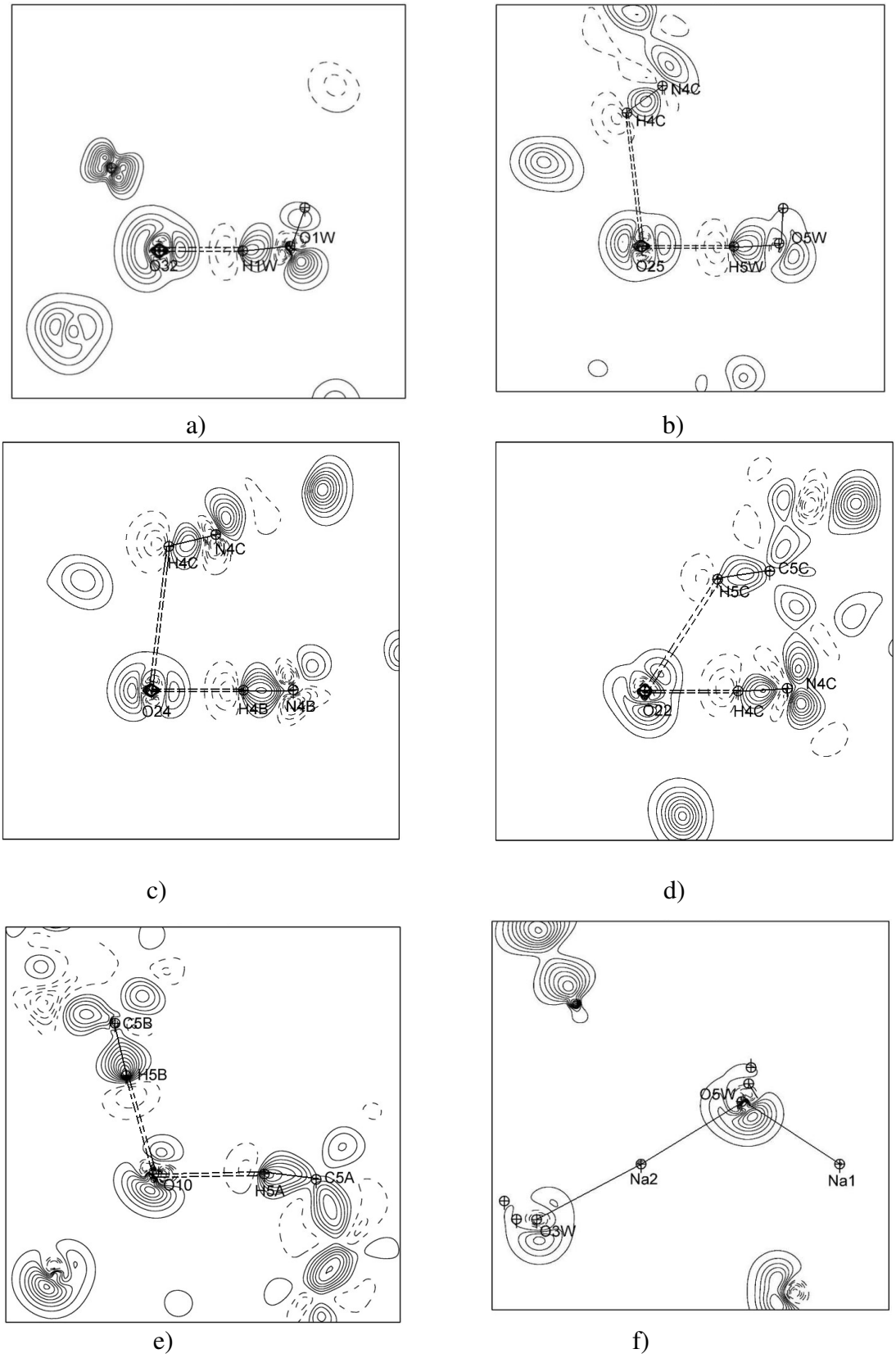
O1W
O32
H1W
a)
N4C
H4C
O5W
O25
H5W
b)
H4C
N4C
O24
H4B
N4B
c)
C5C
H5C
N4C
O22
H4C
d)
C5B
H5B
O10
H5A
C5A
e)
O5W
Na2
Na1
O3W
f)

Figure 7.